Massive surface membrane expansion without involvement of classical exocytic mechanisms.

Michael Fine[1], Christopher Bricogne[2], and Donald W. Hilgemann[1]

Author Affiliation:

[1] University of Texas Southwestern Medical Center, Department of Physiology, Dallas, Texas, USA

[2] UCL Cancer Institute, University College London, Gower St, London, UK.

Corresponding author: Donald.Hilgemann@utsouthwestern.edu

Orcid ID: 0000-0002-5288-5133

Abstract

Activation of TMEM16F, a Ca^{2+} -dependent ion channel and lipid scramblase, causes massive surface membrane expansion in multiple cell types by unresolved mechanisms. We describe here that membrane expansion reflects opening of deeply invaginating surface membrane compartments when anionic phospholipids are lost from the cytoplasmic membrane leaflet. Compartments that open contain vesicle-associated membrane proteins (VAMPs) and can open with as little as one micromolar free Ca_i^{2+}. Cationic peptides that sequester anionic phospholipids open the compartments from the cytoplasmic side without Ca^{2+}. Monovalent cations facilitate membrane expansion via coupled permeation with anionic phospholipids through TMEM16F. When monovalent cation concentrations are reduced, membrane expansion can be reversed by changing ion gradients and membrane voltage. Depolarization closes the compartments by generating inward cation gradients through TMEM16F that promote influx of anionic phospholipids. In summary, TMEM16F-mediated membrane expansion likely does not reflect exocytosis but rather the relaxation of constrictions that close surface membrane invaginations.

Introduction

Plasma membrane (PM) dynamics in eukaryotic cells reflect to a large extent the function of exocytosis and endocytosis. In brief, the PM is continuously modified by discrete membrane fusion and excision events that transfer chemicals to and from the extracellular space and modify the protein content of the PM (Sudhof and Rothman, 2009). Beyond the transport of chemicals and membrane proteins, PM expansion can become essential for cell growth (Tojima et al., 2014), to allow cell swelling (Groulx et al., 2006), to repair PM wounds (Togo et al., 1999; Cooper and McNeil, 2015; Corrotte et al., 2015; Moe et al., 2015) , to relax membrane tension from chronic stretch, e.g. bladder extension (Lewis and de Moura, 1984), and to execute multiple steps in mammalian fertilization (Gadella and Evans, 2011).

Both electrical and optical methods have revealed that multiple cell types increase their PM area substantially during large elevations of cytoplasmic Ca^{2+} (Coorssen et al., 1996; Ninomiya et al., 1996; Kasai et al., 1999; Togo et al., 2003; Kreft et al., 2004; Bretscher, 2008; Cohen et al., 2008; Yaradanakul et al., 2008) , up to two-fold within a few seconds in some cell types (Wang and Hilgemann, 2008; Yaradanakul et al., 2008; Bricogne, XXXX). To what extent the various responses occur by a single molecular mechanism remains unclear. Ca^{2+}-activated PM expansion that occurs in fibroblasts is not inhibited by tetanus toxins and does not appear to use synaptotagmins as Ca^{2+} sensors (Wang and Hilgemann, 2008). In contrast to the usual function of synaptotagmins (Sudhof, 2012), PM expansion in fibroblasts has a nearly linear dependence on cytoplasmic Ca^{2+} (Yaradanakul et al., 2008). As described in a companion article (Bricogne, XXXX) , PM expansion in fibroblasts, Jurkat cells, and HEK293 cells can be initiated by the transmembrane protein, TMEM16F (Bricogne, XXXX). When activated by Ca^{2+}, TMEM16F evidently functions simultaneously as a nonselective cation channel and as a phospholipid scramblase (Yang et al., 2012; Suzuki et al., 2013; Fujii et al., 2015; Scudieri et al., 2015) and we analyze here how these functions mediate PM expansion.

To facilitate the presentation of Results, we illustrate our working hypotheses in Fig. 1. As described in the companion article (Bricogne, XXXX), the rate of PM expansion in Jurkat T cells, monitored via membrane capacitance (C_m), mirrors the rise and fall of TMEM16F channel openings, monitored as membrane conductance (G_m). In fact, as shown in Fig. 1A, the integral of the G_m signal ($\int G_m$) can be scaled to match the rising C_m signal. One potential explanation is that TMEM16F activity limits PM expansion, and this is supported by the phenotype of HEK293

cells that overexpress TMEM16F. Wild-type HEK293 cells have a low TMEM16F conductance and expand their PMs to only to a small extent during Ca^{2+} elevations, but overexpression of TMEM16F markedly enhances the PM expansion responses ((Bricogne, XXXX),Fig.5D).

Fig. 1B illustrates how TMEM16F may mediate PM expansion. As documented in Results, the membrane compartments that expand the cell surface can extend quite deeply into cells, and they appear to be constricted in regions where they converge with the outer PM. Both openings and subsequent closings of these compartments are shown to be reversible. This requires that the compartments open without collapse of their structures, similar to proposals for 'kiss-and-run' exocytosis (Alabi and Tsien, 2013; Oleinick et al., 2017; Wen et al., 2017) and dense core exocytosis in chromaffin cells (Fulop et al., 2005). To explain that the compartments can close reversibly, we are forced to suggest that the compartments may be contiguous with the PM both before they open and after they close. As illustrated, this can be explained if the compartments are constricted by membrane proteins that bind anionic phospholipids, thereby isolating them electrically from the extracellular space. Loss of anionic lipids during TMEM16F activity then releases the constrictions and opens the compartments.

To explain TMEM16F function, as described in Results, we propose that TMEM16F exists in three activity states; closed, open and inactive (see Fig. 1C). In the absence of cytoplasmic Ca^{2+}, TMEM16F channels are closed and have no scramblase activity. Upon binding Ca^{2+}, the channels conduct both monovalent cations and phospholipids. Cations are conducted without phospholipids, but monovalent cations must occupy the pore for anionic phospholipids to enter. Monovalent cations and anionic phospholipids then permeate the pore in a coupled, electroneutral fashion. Finally, the close coupling of TMEM16F activity and PM expansion leads us to suggest that TMEM16F inactivates as anionic lipids are lost from the cytoplasmic leaflet. In other words, TMEM16F, like many ion channels, is activated by binding anionic phospholipids at regulatory sites on the cytoplasmic side (Hilgemann et al., 2018), independent of phospholipid binding within the pore. As to the identity of the membrane compartments that open, caveolae (Shaul and Anderson, 1998) may in principle be involved, consistent with the notion that caveolae open and close in a regulated fashion (Anderson et al., 1992). However, the larger, deeply invaginating components to be described are inconsistent with the morphology of caveolae. From previous work on cell wounding and Ca^{2+} signaling, membrane compartments dubbed "enlargeosomes" in a variety of cell types (Cocucci et al., 2007; Cocucci et al., 2008; Racchetti et al., 2012) are most consistent with our morphological analysis.

Results.

We first describe PM expansion morphometrically and demonstrate the presence of specific VAMP proteins in the compartments that open. Then, we present results relevant to the physiology of PM expansion, including Ca^{2+} requirements, dependence on cell confluence in fibroblasts, and PS exposure within deeply invaginating membrane compartments. Next, we describe reversal of PM expansion by extracellular substitution of ions for the disaccharide, trehalose, the activation of PM expansion by cytoplasmic chelation of anionic phospholipid head groups, and the enhancement of PM expansion by sequestering anionic phospholipids in the outer monolayer. Finally, we turn to the molecular function of TMEM16F and demonstrate reversal of PM expansion by manipulating ion gradients and imposing membrane potentials that influence TMEM16F scrambling function. We provide the composition of 5 standard extracellular (Out) and cytoplasmic (In) solutions in Materials and Methods, and relate any further solution modifications to those 10 solutions.

Optical characterization of TMEM16F-mediated PM expansion. In a previous study, we used electron microscopy to attempt to identify the membrane compartments in BHK cells that fuse to the cell surface during Ca^{2+} elevations (Yaradanakul et al., 2008). The number of secretory vesicles found within 500 nM of the PM was >10-fold less than would be required to explain the PM expansion observed. Furthermore, PM expansion did not bring ion transporters such as Na/K pumps and constitutively expressed transporters into the PM. As described in the accompanying article (Bricogne, XXXX), analysis by confocal microscopy reveals no involvement of endoplasmic reticulum or acidified lysosomes in PM expansion. Furthermore, VAMP2 cleavage by tetanus toxins is without effect on PM expansion (Wang and Hilgemann, 2008; Bricogne, XXXX), and neither super-resolution microscopy nor TIRF microscopy reveals a significant role for recycling endosomes in PM expansion.

Given these results, it appeared significant that FM dyes reversibly labelled deep membrane compartments during Ca^{2+} elevations (see Movie 1). Since however FM4-64 fluorescence is not proportional to C_m (Bricogne, XXXX), we required another dye for quantitative analysis. From several dyes tested (Hilgemann and Fine, 2011) we found that the impermeable dye Trypan blue (TB) fulfilled most of our criteria. TB fluorescence increases when it binds PM sugars and proteins (Harrisson et al., 1981) without insertion into the bilayer as occurs with styryl dyes. As shown in Fig. 2A, TB fluorescence remains proportional to C_m during PM expansion and during MEND responses in Jurkat WT and TMEM16F-null cells (Solutions In_1 and Out_1, containing

physiological monovalent cation concentrations; Pearson correlation coefficient, 0.9; slope, 0.96 ±0.03).

Jurkat and HEK293 cells were then patched and labelled with TB, as illustrated in Figs. 2B, and an initial depth of reversible membrane staining was determined (Figs. 2B-2E, indicated in blue). Cells were then washed, cytoplasmic Ca^{2+} was elevated via ionomycin (5 μM) application, and cells were relabelled with TB for a second analysis (Fig. 2B to 2E, indicated in red). As quantified in Figs. 2D and 2E, the increase in labelling that occurs in Wildtype Jurkat and HEK293 cells after Ca^{2+} elevation extends on average 2.6 and 2.1 μm further into the cells than fluorescence in control measurements. TMEM16F-null cells exhibited no change in labelling depth in response to Ca^{2+} elevations (Fig. 2C). Fig. 2F shows results for NCX1.1-expressing BHK cells in which Ca^{2+} elevations can be induced by activation of reverse Na/Ca exchange (NCX) (Yaradanakul et al., 2008). Similar to HEK293 and Jurkat cells, reversible TB fluorescence also extends many microns deep into the cytoplasm of BHK cells after Ca^{2+} elevations. As evident in the micrographs, individual compartments had remarkably large diameters of >1 μm, appear quite distinct from the PM, and appear to be constricted at their interfaces to the outer PM. Nevertheless, TB labelling rapidly reverses upon washout, thereby verifying connectivity to the extracellular space. Together, these results document that most membrane compartments which open during TMEM16F activation extend deeply into cells and are not morphologically consistent with conventional secretory vesicles, caveolae, or lysosomes. Furthermore, the optical results are consistent with large C_m steps (0.1 to 0.5 pF, equivalent to many 100s of secretory vesicles) observed often during PM expansion in fibroblasts (Wang and Hilgemann, 2008).

Confirmation of VAMP proteins in membrane compartments that open. The morphology of the compartments just described is consistent with reports that novel organelles, dubbed enlargeosomes, expand the cell surface during high Ca^{2+} responses in several cell types (Cocucci et al., 2007; Cocucci et al., 2008). The SNARE protein known as vesicular organelle-associated membrane protein_4, VAMP4, was reported to be enriched in those compartments (Cocucci et al., 2008). Therefore, we expressed VAMP2, 4 and 7 constructs with a luminal pHluorin (pHl) fusion in BHK cells to test whether these proteins indeed enter the PM during PM expansion. The TB absorption spectrum is well suited to quench pHl. Therefore, it is expected that upon compartment opening the exposed fluorescent domains will be quenched by extracellular TB. As shown in Fig. 3 (Solutions In_2,and Out_2), TB could indeed be used to determine the initial colocalization of fluorescent signals as well as quenching of any new

VAMP-pHl fluorescence entering the PM during Ca^{2+} elevations. To do so, TB was applied and removed both before and after Ca^{2+} elevations. The PM expansion induced by Ca^{2+} influx (see left column of Fig. 3) amounted in each case to ~50%. Before Ca^{2+} elevation, TB (100 µg/ml) caused strong quenching of both VAMP2 and VAMP7 fluorescence, but no quenching of VAMP4 fluorescence (Fig. 3, far right column). Colocalization of TB fluorescence and pHlourin fluorescence (overlaid after TB washout) revealed that VAMP2 has a prominent PM expression which colocalizes with TB fluorescence and quenches 57% of the pHlourin signal (far right column). VAMP7 also has strong surface expression that colocalizes with TB fluorescence. Approximately 50% of VAMP7 –pHl signal is quenched by TB. VAMP4 has a distinct intracellular fluorescence pattern with no colocalization with TB fluorescence or quench before Ca^{2+} influx.

Subsequent to PM expansion VAMP2 shows very little change in colocalization and pHluorin quenching, while VAMP7 shows a modest increase in both quenching and colocalization. VAMP7-positive punctae are clearly increased by the Ca^{2+} elevation and are quenched by TB after Ca^{2+} stimulation. VAMP4, however, displays the most robust increase in colocalization and quenching, and the compartments expressing TB-accessible VAMP4 clearly extend deeply into cells. (see Movie 3). We conclude that expressed VAMP4 fusion proteins, and to some extent VAMP7 fusion proteins, accumulate in the membrane compartments that expand the PM. We stress however that these results do not indicate a physical involvement of VAMP proteins in PM expansion but simply support the idea that membrane compartments dubbed enlargeosomes participate in PM expansion, as opposed to endosomes, ER, and lysosomes,

PM expansion and lipid scrambling with highly controlled free cytoplasmic Ca^{2+}. Figs. 4 and 5 illustrate experiments using highly Ca^{2+}-buffered pipette solutions, rather than Ca^{2+} influx, to activate TMEM16F via a constant free cytoplasmic Ca^{2+} concentration. Fig. 4 shows the time courses of PM expansion and anionic phospholipid exposure in a BHK cell using 4 µM free Ca^{2+}. (Solutions In_3 with 5 mM EGTA with 4.6 mM Ca^{2+} and Out_2). Membrane area increases by 50% over 10 min, and during this same time the cationic peptide heptalysine-rhodamine (K7r) binds increasingly strongly, but reversibly, to the outer monolayer (Yaradanakul et al., 2008; Bricogne, XXXX). Line scans of the K7r fluorescence illustrate that K7r binding, similar to TB binding, extends deeply into the cell. Movie 2 documents in more detail both the reversibility and depth of K7r binding.

Previously, we described that with acute Ca^{2+} elevations via reverse NCX in BHK cells about 20 μM free Ca^{2+} was required to initiate membrane expansion (Yaradanakul et al., 2008). Given however that NCX currents inactivate and that the Ca^{2+}-dependence of membrane expansion showed little or no cooperativity, we re-examined this issue by systematically reducing the free Ca^{2+} to determine the minimal concentrations needed to drive membrane expansion. In presenting these results, we note first for BHK cells that PM expansion can clearly have a strong dependence on the regulatory state of cells. Using EGTA-buffered solutions with cytoplasmic free Ca^{2+} concentrations of 1 to 5 μM, it is our routine observation that PM expansion does not occur when cells are less than 90% confluent (blue experimental record and error bar in Fig. 5A). Using BHK cells that were 90 to 100% confluent, however (red recordings and error bars in Fig. 5A), PM expansion reaches 40% over 12 min when the cytoplasmic solution is buffered to 1 μM free Ca^{2+} (30 mM EGTA, 20 mM Ca^{2+}, pH 6.9 with no Mg and 2 mM of the nonhydrolyzable ATP analogue, AMPPNP; Solutions In_4 and Out_4). The inclusion of AMPPNP and the absence of Mg in cytoplasmic solutions is expected to hinder most ATPase activities. Thus, the results verify that membrane expansion does not require ATPase activities. Employing spermine (1 mM) in the cytoplasmic solutions to block TMEM16F activity (Bricogne, XXXX), PM expansion with 1 μM free Ca^{2+} was decreased by 80%. While this result reflects block of the TMEM16F pore by polyamine, it will be described in Fig. 7 that higher concentrations of polyamines can promote significant membrane expansion responses in the absence of Ca, probably as a result of chelating anionic phospholipids. In further experiments in this same series, removal of cytoplasmic Ca^{2+} decreased PM expansion to about 10%.

Using Jurkat cells in Fig. 5B, a somewhat higher free Ca^{2+} (3 μM) was required (30 mM EGTA with 27 mM Ca^{2+}, pH 7.0) to elicit reliable a PM expansion of 25%. For unknown reasons, Jurkat cells lost about 18% of their membrane area over 10 min when perfused with Ca^{2+}-free solutions. In TMEM16F-null Jurkat cells, MEND was activated by 3 μM free Ca^{2+} with 30% of the PM being internalized. This is fully consistent with equivalent experiments using ionomycin in TMEM16F-null Jurkat cells (Bricogne, XXXX). From these results, we conclude that the Ca^{2+} requirement for reliable PM expansion is substantially lower than previously estimated, whereby the expansion occurs very slowly with 1 to 3 μM free Ca^{2+}. Furthermore, the results suggest that PM expansion by the mechanisms analysed here may be subject to physiological regulation.

PM expansion by TMEM16F activation is reversible. Next, we address a key mechanistic question of this study, namely whether PM expansion indeed reflects fusion of submembrane vesicles with the cell surface. As described in Figs. 6, 8, 12 and 14, PM expansion in BHK cells is readily and rapidly reversible. As background to Fig. 6, disaccharides are known to decrease the lateral mobility of phospholipids in membrane bilayers (van den Bogaart et al., 2007), and trehalose, in particular, is known to affect physical properties and the functionality of lipid bilayers (Kapla et al., 2013). We reasoned therefore that substitution of ions for trehalose might promote membrane-membrane interactions that close the submembrane compartments. When trehalose was substituted for ions in our standard solutions (Solution In_3 and Out_2 versus Out_5), PM expansion induced by reverse NCX activity was decreased within 4 s by 75% of the maximal PM expansion that occurred during Ca^{2+} influx (n=9). Usually, the compartments remained closed after removal of trehalose. The fact that PM expansion can be rapidly reversed suggests that membrane fusion, if it is occurring, is not complete. In this connection, we remind that hypertonic solutions reliably cause exocytosis in most synapses in the absence of Ca^{2+}, and this observations has been exploited extensively to study exocytosis (Stevens and Williams, 2000). Using similar protocols with hypertonic solutions in BHK and Jurkat cells, however, we have never activated signficant PM expansion (n>10), suggesting that the PM expansion described here operates by different principles from exocytosis.

Polycations activate PM expansion from the cytoplasmic side. We next considered the role of phospholipids in TMEM16F-induced membrane expansion. We hypothesised that anionic phospholipids in the cytoplasmic leaflet could be attachment sites for proteins that hold membrane compartments closed. Accordingly, the scrambling activity of TMEM16F would release the constrictions that close these compartments and open them to the extracellular space. Accordingly, sequestration of anionic phospholipids by cationic peptides, proteins and other polycations should release the constrictions and trigger membrane expansion. In the experiments described in Fig. 7, the cytoplasmic solution contained 10 mM EGTA with no added Ca^{2+}, no added Mg, no ATP, and no GTP (Solutions In_5 and Out_4). As shown in Fig. 7A, C_m increased over 5 min by 40% when BHK cells were opened in the presence of 3 mg/ml protamine, a cationic protein that binds avidly negatively charged phospholipids of biological membranes (Ichev et al., 1985) and reverses the anticoagulant effects of heparin (Carr and Silverman, 1999). As shown in Fig. 7B, C_m increased over 5 min by 37% when BHK cells were opened in the presence of 0.1 mM K7r in the cytoplasmic solution. As shown in Fig. 7C, spermidine (3 mM) was partially effective in BHK cells, increasing C_m by ~10%, and as shown in

Fig. 7C, C_m increased by 37% over 2 min when Jurkat cells were opened in the presence of 3 mg/ml protamine.

PS gradients can drive forward and reverse PM expansion. The experiments just described lend initial support to the idea that loss of negatively charged lipids from the cytoplasmic membrane leaflet, rather than a gain of negatively charged lipids in the outer monolayer, mediates the opening of membrane compartments. Further key predictions are that, when TMEM16F is active, an enrichment of PS in the extracellular monolayer should favour compartment closure, while chelation of PS on the extracellular side should shift PS from the cytoplasmic side to the extracellular side and thereby favour PM expansion.

As outlined in Fig. 8A, we enriched cells with PS by applying PS-albumin complexes prepared in a 1:2 ratio (Bartholow and Geyer, 1982) by sonication of PS with albumin in distilled water. Using cytoplasmic solutions with 3 μM free cytoplasmic Ca^{2+} (20 mM EGTA with18 mM Ca^{2+}), PM expansion amounted to 35% on average in 5 experiments. Application of 120 μM albumin with 60 μM PS then resulted in complete reversal of PM expansion after a delay 3 to 4 min. In fact, C_m values decreased significantly below baseline, as expected if PS activates significant endocytic responses in addition to reversing PM expansion. We note that other anionic phospholipids, especially PIP_2, can promote endocytic processes when perfused into cells (Lariccia et al., 2011).

Figure 8B demonstrates that sequestration of anionic phospholipids on the extracellular side promotes PM expansion. In these experiments, we used Na/Ca exchangers to generate Ca^{2+} influx in BHK cells. We then compared PM expansion in the presence and the absence of 3 mg/mL extracellular protamine (Solution In_3 and Out_2). PM expansion during application of 1 mM extracellular Ca^{2+} for 2 min amounted to 40% and was increased to 80% (p=0.02) in the presence of extracellular protamine. Importantly, peak NCX currents were unchanged. In summary, extracellular PS can reverse Ca^{2+} -induced PM expansion in BHK cells, albeit with a delay, while chelation of extracellular PS can promote markedly PM expansion as expected of PS is in rapid equilibrium between monolayers during Ca^{2+} elevations.

Relationships between TMEM16F conductance and PM expansion. We analyze next the specific relationships between monovalent cation concentrations, ion permeation, and PM expansion during TMEM16F activation. Fig. 9 describes results for Jurkat cells in which PM expansion was monitored via capacitance (C_m) changes, and membrane current (I_m) and conductance (G_m) were monitored in parallel. Ca^{2+} elevations were induced by ionomycin (5

μM) application in the presence of 2 mM Ca^{2+} for to 1 min. As shown in Fig. 9A (Solutions In_1 and Out_1), the time course with which C_m rises follows closely the time course of membrane current (I_m) and conductance (G_m). Specifically, the integral of the G_m signal corresponds to the time course of the C_m signal, after scaling, and the derivative of the C_m signal corresponds to the time course of the G_m signal after scaling (>20 observations). Given this close relationship, we next tested whether TMEM16F conduction of ions per se controls PM expansion. To do so, we replaced cytoplasmic and extracellular ions with aspartate (Asp=As), *N*-methyl-d-glucamine (NMG=Nm), or isoosmotic sucrose (Suc) (Fig. 9B; Solutions In_3 and Out_2). The presence of either cytoplasmic Na (40 mM in Fig. 9B) or K supported large-scale PM expansion in the absence of Cl, while expansion responses were smaller without Na or K on the cytoplasmic side but with NaCl outside. Responses were reduced by ~50% from control responses when Na and K were replaced with equimolar NMG-Asp on both membrane sides, and they were reduced by 80% when TEA-As was employed on both membrane sides. Replacement of 90% of ions with isotonic sucrose fully blocked exocytosis.

The relative changes of PM expansion with different ions correspond roughly to the relative TMEM16F permeabilities to Na, K, NMG, and TEA (Yang et al., 2012). Therefore, we tested whether PM expansion is influenced by ion permeation per se. Fig. 9C illustrates experiments in which we employed an outwardly directed Na gradient (30 mM cytoplasmic Na with 110 mM cytoplasmic NMG and 140 mM extracellular NMG), so that TMEM16F current became strongly voltage dependent. From the experiments of Fig. 9B, it may be assumed that PM expansion in this condition is limited in rate and extent by the cytoplasmic Na concentration. In contrast to results with equal K and Na concentration on opposite membrane sides (Fig.9A), large (>0.5 nA) outward Na currents are generated in these experiments (Fig. 9D green). Holding membrane potential at +50 mV, ionomycin causes a large transient conductance, as in Fig. 9A, which develops and decays with the same time course as PM expansion (Fig.9C top and Fig. 9D blue). When membrane potential is held at -50 mV, both the conductance and outward membrane currents are strongly suppressed. Nevertheless, PM expansion proceeds to the same extent (ΔC_m) and with the same maximal rate ($\Delta C_m/dt$) as at +50 mV (Fig. 9C-D red). Composite results (n=6) shown in Fig. 9D therefore dissociate ion conduction *per se* from PM expansion. The results also negate a possibility that Ca^{2+} influx via TMEM16F initiates PM expansion because, in that case, hyperpolarization would enhance Ca^{2+} influx and thereby PM expansion. Rather, another function of TMEM16F must underlie the activation of PM expansion.

Anionic phospholipid scrambling and PM expansion require monovalent cations. As outlined in the Introduction, our further experiments suggest that monovalent cations must occupy the TMEM16F pore before anionic phospholipids can enter and permeate the pore (see Fig. 1). Permeation of anionic phospholipids then can take place in an electroneutral fashion that is not influenced by membrane voltage. To explain this suggestion, we provide in Fig. 10 simple simulations of the working hypotheses, assuming for simplicity that TEA cannot occupy the TMEM16F pore and that Na, K and Cs occupy the pore with equal affinity. Simulation details are provided in Material and Methods. Each black curve in the Fig. 10 depicts the fractions of invaginating membrane compartments predicted to be open (F_{open}) as a result of anionic phospholipids being lost from the cytoplasmic to the extracellular leaflet. It is assumed that 4 phosphatidylserine (PS) molecules are bound by membrane proteins to close the compartments, and it is assumed that PS binding is half-saturated at approximately the resting concentration of PS in the inner monolayer (i.e. with100 arbitrary PS units). Here and for subsequent simulation results, we assume that PS has a 4-fold higher affinity for the outer monolayer than for the inner monolayer. This is justified by the fact that the outer monolayer is more ordered than the inner monolayer, resulting in 5-times slower diffusion of phospholipids in the outer monolayer than in the inner monolayers (Cribier et al., 1990). As a result of this assumption, the majority of PS translocates to the outer monolayer during TMEM16F activation.

Three simulations are presented in Fig. 10, one with a purely outward cation gradient (A), one with a purely inward cation gradient (B), and one upon switching monovalent cation gradients from outward to inward (C). In Fig. 10A the cytoplasm is assumed to contain 140 mM of monovalent cation (X) while the extracellular solution contains 140 TEA (i.e. no TMEM16F-interacting cations). Upon increasing cytoplasmic free Ca^{2+} in a step from 0 to 20 μM, the fractional opening of invaginating membrane compartments (F_{open}) increases from <0.1 to nearly 1 within 10 s, TMEM16F generates an outward current that inactivates as PS is lost from the cytoplasmic side, and the amount of PS in the cytoplasmic leaflet decreases from nearly 100% of the PM PS to about 15%. The cartoon below the simulation illustrates the partial reactions that scramble PS under these conditions and that occurs in a completely electroneutral fashion. When a cation binds to the cytoplasmic end of the pore (#1), a PS molecule can bind from the cytoplasmic side (#2), the cation and PS can traverse the pore (#3), PS can move from the pore to the outer monolayer (#4), and the cation can exit the pore (#5). As illustrated in Fig. 10B, TMEM16F according to our model cannot scramble anionic phospholipids in the absence of permeable monovalent cations. When permeable extracellular cations are applied, an inward

cation current is generated. As cations reach the inner mouth of the pore, they support the movement PS to the extracellular side. As illustrated in the cartoon below the simulation, the cycle of reactions moves one negative charge outwardly per cycle, and this reaction cycle can be stimulated by hyperpolarization. Fig. 10C illustrates the induction of reverse PS scrambling. Initially, it is assumed here that the cytoplasm contains 20 mM permeant cations while the extracellular solution contains no permeant cations. Over time, the majority of PS reaches the extracellular monolayer and accumulates in the outer monolayer as a result of its higher affinity for PS than the inner monolayer. When 140 mM permeant cations are applied to the outside at an early time point, scrambling is stabilized at an intermediate level. If PS is allowed to accumulate further in the outer monolayer, application of extracellular permeant cations can partially reverse scrambling via the reaction sequence illustrated in the cartoon for reverse electroneutral transport.

Figures 11 and 12 illustrate each of these model predictions by experiments. Fig. 11 shows the activation of scrambling and PM expansion when experiments are initiated without permeant cations on the cytoplasmic side. A free cytoplasmic Ca^{2+} concentration of 5 μM was employed with, at first, 140 mM TEA on both membrane sides. PS exposure was monitored via periodic application of K7r and measurement of its membrane-associated fluorescence. After 3 min in the presence of TEA on both membrane sides, C_m remains stable and the K7r signal remains small and stable. After substituting extracellular TEA for Cs (140 mM; Solution Out_3), however, C_m begins to rise with a delay of about 30 s, and total PM expansion amounts to 80% at 10 min. The reversible K7r signal grows roughly in proportion to membrane area, and reveals reversible binding of K7r into compartments that extend multiple microns into the cell (see micrograph #3).

Figure 12 illustrates further predictions of simulations by experiments in which either extracellular Na (Figs. 12A and 12B) or extracellular Cs (Figs. 12C and 12D) were used to slow and/or reverse PM expansion (Solutions In_5 and Out_4). Cytoplasmic free Ca^{2+} was heavily buffered with 30 mM EGTA to 3 μM (30 mM EGTA/27 mM Ca^{2+}). Fig. 12A illustrates the case in which PM expansion is initiated with a low cytoplasmic cation concentration (20 mM Na) with 140 mM extracellular TEA. Substitution of TEA for 140 mM Na on the outside effectively stops PM expansion, as in the 2nd simulation in Fig. 10C. Fig. 12B illustrates records in which PM expansion is allowed to proceed to nearly its maximal extent with 3 μM free Ca^{2+} (as in curve #4 in Fig. 10C). In this case, PM expansion reverses by about 25% upon substituting extracellular TEA for Na, and expansion can be reactivated by the reverse concentration change. Using Cs as a substitute for TEA in Fig. 12C, Cs initially stops PM expansion at an intermediate value, as

in Fig. 12A with Na. After expansion is allowed to proceed further in the presence of TEA, Cs causes an approximately 25% reversal of PM expansion, equivalent to 10% of total membrane area, similar to results for extracellular Na in Fig. 12B. Fig. 12D illustrates in more detail the speed with which membrane area changes can be reversed by applying and removing Cs in these experiments. The maximal rates of membrane area change become established within just a few seconds after changing the extracellular solution composition. We mention that, in individual experiments, the rates of membrane area change required up to 30 s to change after changing solutions, perhaps because intracellular cation concentrations can change significantly during these experiments and require time to readjust after changing concentration.

PM expansion can be reversed by depolarization. Finally, we consider effects of membrane potential on nionic lipid scrambling and PM expansion with the aid of simulations. With physiological ion concentrations on both membrane sides, simulations predict no effect of membrane potential because the TMEM16F channel is nearly saturated with cations. This is illustrated in Fig. 13A (140 mM monovalent cations on both membrane sides; dissociation constant, 15 mM at both channel orifices). Voltage changes from -70 to +70 mV have no effect on PS scrambling or compartment opening, as described experimentally in Fig. 9A. Fig. 13B illustrates simulations for an outward cation gradient 40 mM permeant cation on the cytoplasmic side and no permeant cation on the outside, equivalent to experiments presented in Fig. 9B. Voltage changes from -70 to +70 mV are nearly without effect because cytoplasmic pore sites are nearly saturated and because PS binds with higher affinity in the extracellular than in the cytoplasmic monolayer. Owing to this asymmetry of affinities, voltage must be increased to >120 mV to significantly drive and electrogenic reverse flux of PS.

As expected, membrane potential effects become significant when permeant cation concentrations are reduced to dissociation constant of the channel pore. As shown in Fig. 13A with 10 mM permeant monovalent cations on both membrane sides, the fraction of open compartments (F_{open}) increases and decreases about 20% during hyperpolarization to -70 mV versus depolarization to +70 mV. The effects are still not particularly large, and Fig. 13D illustrates optimal conditions for effects of membrane voltage. Specifically, the presence of a rather low concentration of permeant cations (2 mM) in the cytoplasm and a relatively high cation concentration (70 mM) on the extracellular side is optimal to make scrambling voltage dependent in the context of other assumptions. Hyperpolarization then strongly favors electrogenic forward PS transport, and therefore membrane compartment opening, while

depolarization negates the electrogenic mode and favors electroneutral reverse mode, thereby favouring closure of PS-dependent membrane compartments.

Figure 14 presents the equivalent experiments employing the conditions just outlined (5 mM cytoplasmic Cs with 70 mM extracellular Cs). We included 2 mM AMPPNP on the cytoplasmic side to block most ATPase activities. Using 5 mM EGTA with 4.5 mM Ca^{2+} (~4 μM free Ca^{2+}), membrane area expands in a progressively accelerating fashion at -30 mV and reaches 130% of control area after 5 min. Upon switching membrane potential to +50 mV, membrane area immediately begins to decline at nearly the opposite rate (~30% per minute) and declines nearly to baseline. In all experiments, these responses could be repeated at least once, and often multiple times, to nearly the same extent as the initial responses. The reversible nature of PM expansion in these experiments indicates that membrane fusion events, if they are occurring, are reversible. Alternatively, the opening and closing of invaginating membrane compartments does not involve membrane fusion and excision events but rather reflects a constriction and relaxation of the compartments, adequate to isolate them electrically from the extracellular space.

Discussion.

It has long been known that many cell types can expand their PM by a large amount in response to elevations of cytoplasmic Ca^{2+} (Coorssen et al., 1996; Ninomiya et al., 1996; Kasai et al., 1999; Togo et al., 2003; Kreft et al., 2004; Bretscher, 2008; Cohen et al., 2008; Yaradanakul et al., 2008), and this expansion has often been suggested to mediate repair of membrane wounds (Togo et al., 2003; Bradke et al., 2012; Cooper and McNeil, 2015; Corrotte et al., 2015) In a companion article (Bricogne, XXXX) we have shown that TMEM16F can initiate PM expansion in multiple cell types. Here we have demonstrated that PM expansion is kinetically and mechanistically coupled to scrambling of anionic phospholipids, which in turn requires occupation of the TMEM16F pore by monovalent cations. Clearly, the underlying mechanisms are substantially different from classical Ca^{2+}-activated exocytosis. PM expansion described here reflects the opening of deeply invaginating PM compartments. We suggest that the openings are regulated by constrictions in junctional regions close to the cell surface.

PM expansion may not involve *bona fide* membrane fusion events. Our results show a very close correlation between the opening of TMEM16F channels and the expansion of the PM in Jurkat cells (Fig. 9). The time course of TMEM16F conductance changes matches closely the time course of PM expansion. Specifically, the integral of conductance signals matches the rising capacitance waveform, as if TMEM16F channel activity directly controls PM expansion. Although cytoplasmic monovalent cations are required for PM expansion (Figs. 9 and 11), ion conduction per se can be entirely dissociated from PM expansion by changing the membrane holding potential (Fig. 9). Rather, it appears that monovalent cations serve as counter charges during the movement of anionic phospholipids through TMEM16F. This requirement would be reasonably explained by the existence of negative charges in the TMEM16F pore that facilitate cation conduction while, at least to some extent, repelling anions and especially anionic phospholipids. The parallel block of TMEM16F conductance and PM expansion by spermine ((Bricogne, XXXX), Fig. 3), possibly as a result of polyamine binding within the negatively charged pore, is also consistent with lipids and ions moving through the TMEM16F channel in a concerted fashion. To what extent polyamines also inhibit TMEM16F activity by sequestering anionic phospholipid into nanodomains (Denisov et al., 1998), and thereby promoting TMEM16F inactivation, is not certain. At substantially higher concentrations than required to block TMEM16F activity, polyamines can promote membrane expansion in the absence of Ca^{2+} (Fig. 7), albeit to a lesser extent than cationic peptides and proteins.

The similar time courses with which PM expands and extracellular K7r binding capacity increases (Figs. 4 and 11) are suggestive of a simple relationship between PS translocation and compartment opening. This impression may be to some extent fortuitous because K7r will simultaneously bind multiple anionic phospholipids (Denisov et al., 1998) and, as represented in our simulations, closure of the membrane compartments likely requires binding of multiple anionic phospholipids by membrane-interacting proteins. Most importantly, we have documented that PM expansion caused by activation of TMEM16F can be partially or completely reversed by establishing large inward cation gradients and by membrane depolarization (Fig. 9 and 11). These results are inconsistent with the idea that PM expansion is occurring via genuine membrane fusion events. Either the fusion events are incomplete and impeded at some step, or else there are no fusion events. The major possibility that emerges is that PM expansion during TMEM16F activation involves membrane that is contiguous with the PM yet uncoupled electrically from the extracellular space. As PS is depleted from the inner monolayer, constrictions in junctional regions of these compartments relax and allow access to the extracellular space.

The membrane compartment that opens. The membrane that expands the PM is clearly not a classical membrane compartment. As stressed throughout this article, expansion involves extended, deeply invaginating membranes that have dimensions of several microns in length and breadth (Figs. 2 and 3). Possibly, therefore the compartment might have been confused with ER in electron microscopy studies. That said, we cannot exclude at this time that caveolae become involved in PM expansion. The assembly of caveolae is highly dependent on PS (Hirama et al., 2017). Experiments described in the companion article (Bricogne, XXXX) effectively eliminate roles for recycling endosomes, endoplasmic reticulum, and lysosomes. The appearance of the vesicle membrane protein, VAMP4, in the PM during PM expansion confirms a previous report (Cocucci et al., 2008) but does not add substantively our understanding of this compartment or for that matter the role of SNARE proteins in PM expansion. Importantly, the membrane that opens does not contain PM ion transporters or ion channels that are otherwise abundant in the PM (Yaradanakul et al., 2008). Finally, we stress that our experiments give no hint whether this membrane might play a role in membrane repair. PM expansion, as described here, could in principle play all the same biological roles played by conventional exocytosis.

The hypothesis that PM expansion reflects relaxation of membrane binding proteins that constrict the necks of these compartments is supported by the following evidence: (1) PM expansion is reversible as expected for a direct dependence on protein binding to anionic

phospholipids (Figs. 9, 11, and 13). (2) Large-scale PM expansion can be initiated in the complete absence of cytoplasmic Ca^{2+} by 'sequestering' anionic phospholipids with cytoplasmic peptides or proteins that bind their head groups with substantial affinity (Fig. 12). (3) PM expansion can be reversed by increasing the PS content of the PM via application of PS-albumin complexes from the outside of the cell, and this occurs specifically under conditions in which TMEM16F activity should be substantial. (4) PM expansion is enhanced by incubating cells with proteins, e.g. protamine, or peptides, K7r, that bind anionic phospholipids and therefore will shift the equilibrium of PS from the cytoplasmic to the extracellular PM monolayer (Fig. 13).

The major open question is the identity of the membrane proteins that mediate membrane constriction, and obvious candidates at this time include (1) dynamins (Schmid et al., 1998; Antonny et al., 2016), (2) BAR domains (McMahon and Boucrot, 2015; Suetsugu, 2016; Salzer et al., 2017), and dysferlins (Demonbreun and McNally, 2016). For now, we have no reason to favour one system over another. Each of these membrane-shaping systems could allow regulation of PM expansion by molecular mechanisms besides phospholipid scrambling, as each of these systems is known to be regulated by factors besides binding to anionic lipids. In this sense, loss of anionic lipids to the extracellular leaflet is likely to be one of many mechanisms that will regulate this form of PM expansion. Thus, cells that do not express TMEM16F may nevertheless use the PM expansion mechanism described here. In this connection, the genesis of the invaginations that open during PM expansion is a key problem for future research. The biogenesis of these compartments might occur via trafficking and fusion of endosomes to pre-existing structures at the PM, and our TIRF analysis is consistent with the idea that recycling endosomes can to some extent fuse to the compartments that open (Bricogne, XXXX). Expansion might also occur via the slow internalization of surface bilayer through the restrictions that hold the compartments closed. Integral membrane proteins would presumably not pass through the constrictions and remain in the outer PM, thereby explaining the relative lack of typical PM transporters and channels in the compartments that open (Yaradanakul et al., 2008).

Physiological roles of constriction-dependent PM expansion. As suggested above, the potential physiological roles of PM expansion without membrane fusion events include all of the same physiological roles attributed to exocytosis. That is to say, this form of PM expansion can mediate the release of cytokines and other chemicals to the extracellular space, can bring new membrane proteins into the cell surface, and can expand the cell surface so as to allow cell

growth and/or swelling. Expansion can occur with as little as 1 micromolar free Ca^{2+} (Fig. 5). It might occur without no requirement for Ca^{2+} if the membrane binding proteins involved are regulated by Ca^{2+}-independent mechanisms. It is possible and indeed likely that some descriptions of PM expansion in the literature, especially electrophysiological descriptions, will be attributable to the processes described here, rather than to genuine exocytic events. It will be of great interest to test whether similar membrane compartments exist in cells that do not express TMEM16F, for example by testing whether cytoplasmic application of polycations opens new PM compartments. Finally, it will be of great interest to determine in which physiological processes this unexpected form of PM expansion plays functionally important roles.

Acknowledgments

We thank Mei-Jung Lin for technical help and discussion. CB was supported by The Rosetrees Trust (M155), MRC Doctoral Training Grant (1132770), and the UCL Bogue Fellowship. DH and MF were supported by National Institutes of Health, USA (HL119843, T32DK007257).

Materials and Methods

Methods were as in the accompanying article (Bricogne, XXXX). Baby hamster kidney (BHK) cells expressing cardiac NCX1 were grown as described (Yaradanakul et al., 2008). Cells were imaged using the Nikon EZ-C1 confocal microscopy system as described in the companion article (Bricogne, XXXX) and in the text. Fluorescent line scans were determined by subtracting the equivalent background fluorescence. Membrane fluorescence depth in microns was determined from line scan images and quantified in ImageJ using 4 distinct membrane regions per cell.

Solutions. Table 1 provides the compositions of major solutions employed. Further solution modifications are given with reference to these solutions in Results.

Solutions (mM)	**Cytoplasmic ("In")**					**Extracellular ("Out")**				
	#1	**#2**	**#3**	**#4**	**#5**	**#1**	**#2**	**#3**	**#4**	**#5**
Dextrose	0	0	0	0	0	10	0	0	0	0
HEPES	10	20	20	30	20	10	10	10	10	10
KOH	140	0	140	160	0	5	0	0	0	0
NaOH	5	40	0	0	20	130	0	0	0	0
CsOH	0	0	0	0	0	0	0	140	0	0
TEA-OH	0	20	0	0	120	0	20	0	140	0
NMG	0	80	0	0	0	0	120	0	0	0
EGTA	0.5	0.5	5	30	30	0	0.5	0.5	0.5	0.5
$CaCO_3$	0	0	0	20	25	0	0	0	0	0
$CaCl_2$	0.25	0.25	4.6	0	0	0	0	0	0	0
$MgCl_2$	0.5	0.5	0.5	0	0	4	4	4	4	4
Aspartate	0	115	125	90	125	0	125	125	125	0
HCl	145	0	0	0	0	135	0	0	0	0
Trehalose	0	0	0	0	0	0	0	0	0	300
pH	7.0	7.0	7.0	7.0	7.0	7.0	7.4	7.4	7.4	7.4

Table 1.

Reagents. Unless stated otherwise, reagents were from Sigma-Aldrich and were the highest available grade. 5 μM ionomycin free acid (Calbiochem) was used unless otherwise stated. Other reagents used were 5 μM FM 4-64 (Life Technologies), 50-500 μM spermine (Sigma-

Aldrich), and 100µg/ml (0.01%) Trypan Blue (Sigma-Aldrich). Rhodamine-conjugated hepta-lysine (rhodamine-KKKKKKK-amide; K7) was prepared by Multiple Peptide Systems (NeoMPS, Inc.).

Simulation of TMEM16F function and deep membrane compartments (Figs. 8 and 10). Simulations of the working hypotheses, presented in Fig. 1, were written in Matlab. The fraction of TMEM16F channels that has no bound Ca is 'F_{closed}', the fraction that has no bound PS at regulatory sites is called '$F_{inactive}$', and the doubly inactivated fraction (F_{closed}•$F_{inactive}$) is not depicted in Fig. 1. The fraction of TMEM16F channels that is open (F_{active}) can translocate cations via two-site pore, and can bind and translocate anionic phospholipids (PS) only when a cation is available at the relevant pore entrance.

In the initial state of all simulation, all PS (PS_{tot}, 100 units) is assumed to be cytoplasmic:
(1) PS_i=100, and PS in the outer monolayer (PS_o) is
(2) $PS_o=PS_{tot}-PS_i$

At any time, the fraction of active TMEM16F channels (F_{active}, see Fig. 1B) is dependent on Ca^{2+} binding to a single TMEM16F site with a K_{50} of 20 µM and the binding of two PS molecules at regulatory sites. Total PS content of the membrane is always 100 PS units. The K_{50} for PS binding to activate TMEM16F is 120 PS units and the Hill slope is 2 (see Fig. 1B), implying that all TMEM16F channels are not activated by the normal PS content of the inner PM monolayer. Thus, the fraction of active TMEM16F channels (F_{active}) is:

(3) $F_{active}=Ca_i/(Ca_i+20\mu M) \cdot PS_i^2/(PS_i^2+120^2)$

The active state (F_{active}) is then subdivided into conducting channels that have no PS bound within their open pores (E_o), channels that have one PS bound within the pore on the cytoplasmic side (E_1), and that have one PS bound within the pore on the extracellular side (E_2). For simplicity, dual PS occupancy is not allowed in the simulations.

The rates of PS translocation in TMEM16F (K_{PSx}), PS binding by TMEM16F (K_{PSon}) and dissociation from TMEM16F (K_{PSoff}) are as follows, relevant to the total PS population of 100:
(4) $K_{PSx}=20\ s^{-1}$
(5) $K_{PSon}=75\ PS^{-1}\bullet s^{-1}$;

(6) K_{PSoff}=400 s^{-1}

To simulate ion translocation within open TMEM16F channels, the E_0 fraction of the F_{active} fraction of TMEM16F (see cation permeation model in Fig. 1), a two-site model is employed with all voltage dependence placed on ion translocation between inner and outer pore binding sites. The rates of ion binding (K_{on}), dissociation (K_{off}), and translocation between occupancy sites (K_x) were assigned relative to a translocation rate (K_x) of 1 s^{-1}. K_{on} is 0.2 $mM^{-1}s^{-1}$ and K_{off} was 5 s^{-1}. When changes of membrane potential (E_m) were simulated, K_x was modified by a single, symmetrical barrier function,

(7) $K_{em} = e^{(0.5 \cdot Em/26mV)}$.

With internal (X_i) and external (X_o) cation concentrations in mM, calculation of TMEM16F ion occupancy states and permeation rates proceed as follows (see Fig. 1B):

(8) $K_1=X_o \bullet K_{on}$

(9) $K_2=K_{off}$

(10) $K_3= K_{off}$

(11) $K_4=X_i \bullet K_{on}$

(12) $K_5= K_{off}$

(13) $K_6=X_o \bullet K_{on}$

(14) $K_7=X_i \bullet K_{on}$

(15) $K_8= K_{off}$

(16) $K_9=K_x \bullet K_{em}$

(17) $K_{10}=K_x/K_{em}$

Using a King-Altman procedure (Lam and Priest, 1972) to calculate occupancy of the four permeation states,

(18) $X_1=K_2 \bullet K_4 \bullet (K_7+K_6)+K_5 \bullet K_7 \bullet (K_2+K_3)+K_{10} \bullet (K_2+K_3) \bullet (K_7+K_6)$

(19) $X_2=K_1 \bullet K_7 \bullet (K_4+K_5)+K_4 \bullet K_6 \bullet (K_1+K_8)+(K_{10} \bullet K_1+K_9 \bullet K_4) \bullet (K_7+K_6)$

(20) $X_3=K_1 \bullet K_3 \bullet (K_7+K_6)+K_8 \bullet K_6 \bullet (K_2+K_3)+K_9 \bullet (K_6+K_7) \bullet (K_3+K_2)$

(21) $X_4=K_2 \bullet K_8 \bullet (K_4+K_5)+K_3 \bullet K_5 \bullet (K_1+K_8)+(K_9 . K_5+K_{10} \bullet K_8) \bullet (K_3+K_2)$

With $S=X_1+X_2+X_3+X_4$, the fractional occupancies of the four states are:

(22) $F_1=X_1/S$, $F_2=X_2/S$, $F_3=X_3/S$ and $F_4=X_4/S$, where F_1 is occupied on the cytoplasmic side by 1 cation, F_2 by two cations, F_3 by a cation on the extracellular side, and F_4 is unoccupied. The (relative) permeation rate (R_{net}) is then:

(23) $R_{net}=F_3 \bullet K_{10}-F_1 \bullet K_9$

Next, the active TMEM16F states with PS bound to the inner (E_1) and outer (E_2) pore binding sites are integrated over time. Assuming that PS can bind from the cytoplasmic side to all E_0 states with cations occupying the cytoplasmic site (i.e. F1 + F2 states), assigning K_{PSon} (75 PS^{-1} •s^{-1}) as the second order rate of PS binding, K_{PSoff} as the PS dissociation rate from E_1 states (400 s^{-1}), and K_{PSx} (20 s^{-1}) as the PS translocation rate between PS sites in the pore,

(26) $dE_1/dt= [PS_i \bullet E_0 \bullet F_{active} \bullet K_{PSon} \bullet (F_1+F_2)-E_1 \bullet K_{PSoff}]+(E_2-E_1) \bullet K_{PSx}$.

To simulate the expectation that lipids in the outer monolayer are more ordered and less fluid, we assume that K_{PSon} is two-fold slower and that K_{PSoff} is two-fold faster on the extracellular side:

(27) $dE_2/dt= [PS_o \bullet E_0 \bullet F_{active} \bullet K_{PSon} * (F_3+F_2)/2-E_2 * K_{PSoff} \bullet 2]+(E_1-E_2) \bullet K_{PSx}$.

The fraction of active channels without a PS bound within the pore is calculated:

(28) $E_0=1-E_1-E_2$,

PS changes in the cytoplasmic leaflet (PS_i) are integrated,

(29) $dPS_i/dt = E1 \bullet K_{PSoff} - PS_i \bullet E_0 \bullet K_{PSon} \bullet F_{act} \bullet (F_1 + F_2)$,

PS in the extracellular leaflet is calculated,

(30) $PS_o=PS_{tot}-PS_{i,}$

the relative TMEM16F current is calculated,

(31) $I_{TMEM16F}=R_{net} \bullet F_{active} \bullet E_0$,

and finally, the fraction of deep membrane compartments open to the extracellular space (F_{open}) is calculated. We assume here that 4 PS molecules must be bound by the constricting membrane proteins and that the PS affinity is quite high. The K_{50}, 35 PS units, is less than one-half of the total PS in the inner monolayer:

(32) $F_{open}=35^4/(PS_i^4+35^4)$.

Simulations were carried out in Matlab with accuracy checking to insure that simulation error was less than line-width in the results presented.

Figure Legends.

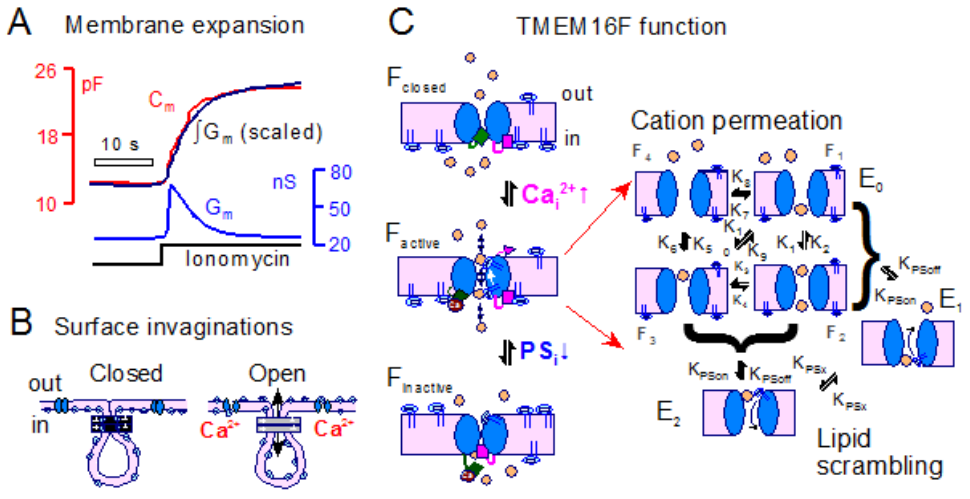

Figure 1. Working hypotheses to account for TMEM16F-mediated PM expansion. (A) Routine recording of membrane capacitance (C_m) and conductance (G_m) changes during a cytoplasmic Ca^{2+} elevation induced by ionomycin (5 μM) with 2 mM extracellular Ca^{2+} in WT Jurkat T-cells. Same conditions as in Fig. 2A-D and Fig. 9. As in >20 similar observations, the wave-form of C_m is superimposable with the integral of the G_m signal. **(B)** Membrane compartments that expand the cell surface extend deeply into cells and are closed by proteins that bind anionic phospholipids, depicted as light blue ovals. Loss of anionic phospholipids from the cytoplasmic leaflet relaxes the constrictions and opens the compartments to the extracellular space. **(C)** TMEM16F channels (blue) are closed (F_{closed}) and do not conduct lipids in the absence of cytoplasmic Ca^{2+}. When cytoplasmic Ca^{2+} rises, TMEM16F binds Ca^{2+} and opens with a nearly linear dependence on Ca^{2+} concentration (F_{active}). Anionic phospholipids can enter the active TMEM16F channels (see expanded diagram) only when a monovalent cation (orange circle) is bound within the channel near the relevant pore opening. Anionic phospholipids permeate the channel together with monovalent cations in an electroneutral fashion. Accordingly, cation gradients can influence the direction of movement of anionic phospholipids. In the presence of ion gradients, lipid scrambling can become voltage dependent in dependence on occupation of the channel by cations. TMEM16F channels enter an inactive state ($F_{inactive}$) when PS is lost from cytoplasmic binding sites. Double inactive states without Ca or PS bound are not depicted. The rates indicated in Fig. 1C, the fractional TMEM16F occupancy by ions (F_1 to F_4), and fractional occupancies by anionic phospholipids (E_0, E_1 and E_2) are used in simulations of Results that are described in Materials and Methods.

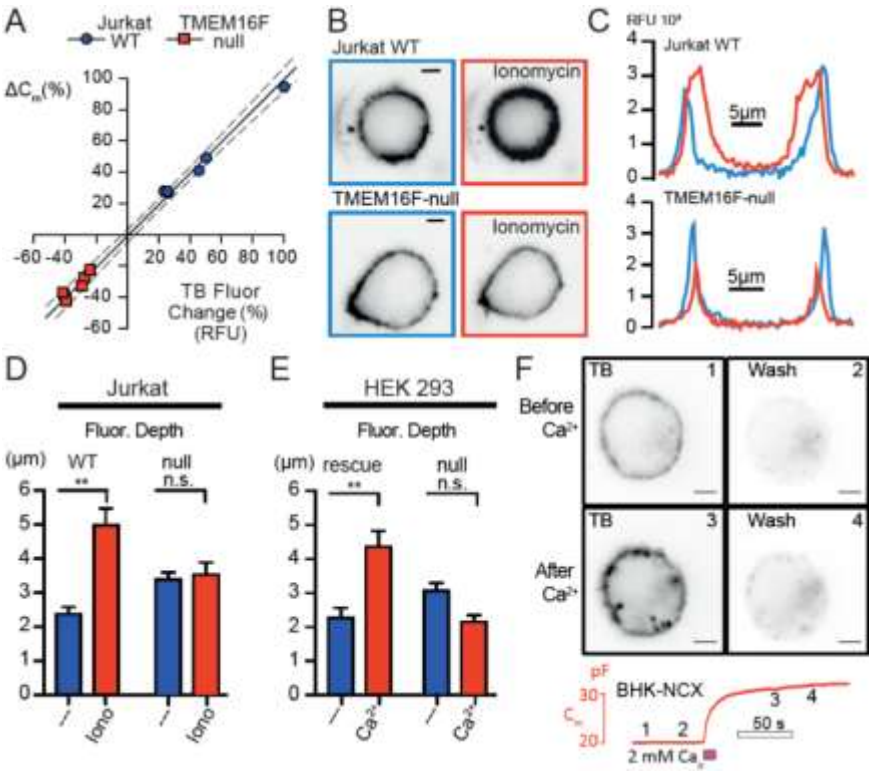

Figure 2. Ionomycin-induced PM expansion involves a membrane compartment that extends deeply into Jurkat, HEK293, and BHK cells. (A) Reversible fluorescent membrane staining using trypan blue (TB, 100 µg/ml) was determined before and after application ionomycin in WT and TMEM16F null Jurkat T-cells. Changes of TB fluorescence (%) are plotted against changes of C_m (%) caused by ionomycin treatment. Linear regression of results with 95% C.I. confirms a linear correlation between TB fluorescence and membrane area (C_m) (PCC=0.9). Images **(B)** and fluorescent line scans **(C)** during application of 100 µg/ml TB in Jurkat WT and TMEM16F-null cells before (blue) and after (red) ionomycin-induced PM expansion. Scale bars are 5µm here and in all subsequent figures. Average membrane fluorescence depth and SEM quantified from **B** for cell lines with and without TMEM16F expression. (**p ≤ 0.01) in Jurkat **(D)** and HEK293 **(E)** cells. Mean values with SEM are given with n>4. **(F)** Confocal imaging a representative BHK cell, with and without TB application, before and after activation of constitutively expressed NCX1.1 by 4 mM extracellular Ca^{2+} with 40 mM cytoplasmic Na. The membrane compartments that expand the cell surface extend several microns into the cell and converge to a "neck"-like structure at the interface to the peripheral membrane surface.

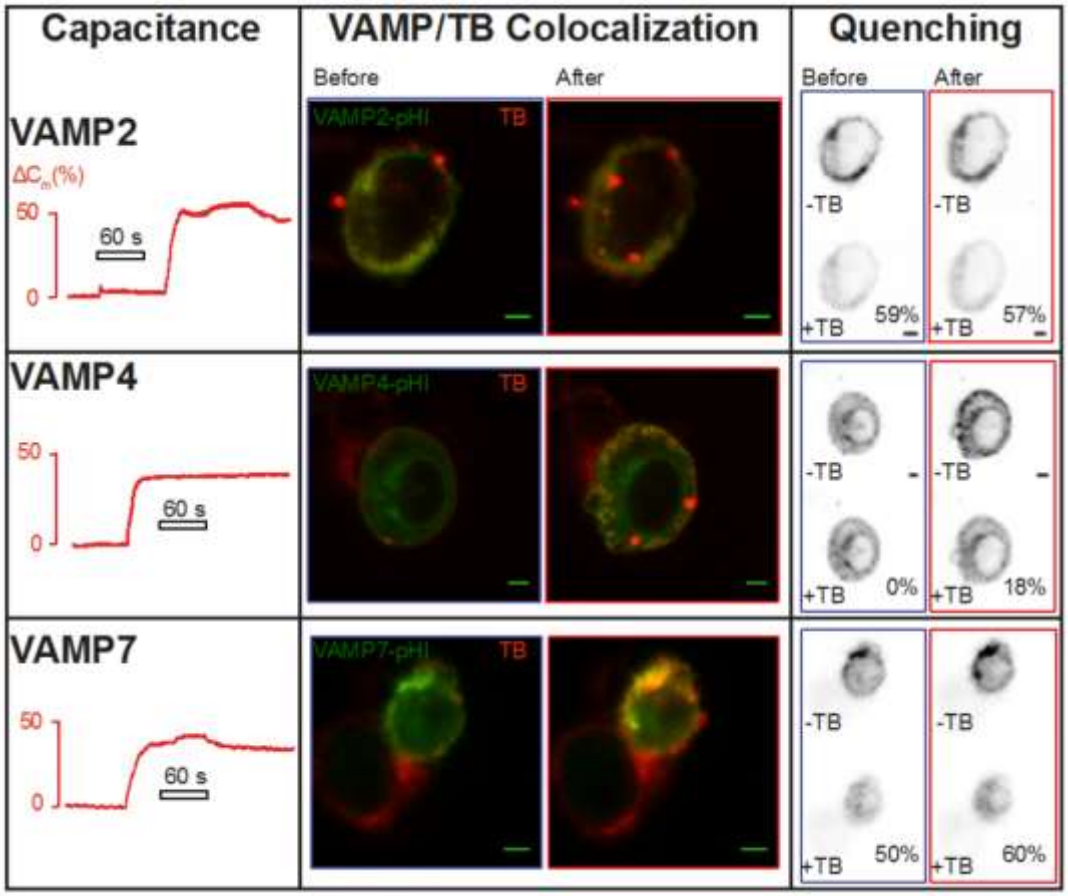

Figure 3. Analysis of VAMP proteins in the PM during PM expansion. Among VAMP2-, VAMP4- and VAMP7- pHlourin (pHl)fusion proteins, VAMP4 fusions preferentially increase cell surface expression after PM expansion. Fluorescence recordings in BHK cells constitutively expressing NCX1.1 and transfected to express green VAMP2, 4, or 7-pHl fusion proteins. Activation of Ca^{2+} influx via NCX causes induces expansion of the PM (left column) corresponding with increases in TB fluorescence (middle column, red).. Colocalization is determined by overlay of TB fluorescence and VAMP-pHl after wash off of TB dye. Quenching is demonstrated by the % loss of pHl signal during TB application (right column). VAMP4-pHl fusion protein accessible to the extracellular space, determined by quench of with TB, is negligible in the control state and increases 18% after PM expansion with corresponding increases in colocalization. VAMP2 is already predominantly expressed at the surface and does not increase further after PM expansion while VAMP7 (also present to some extent at the surface) shows moderate increases in colocalization and an increase in TB quenching of 10%. We stress that the VAMP-containing compartments that open, similar to compartments labelled by dyes, appear to be constricted at their interfaces to the outer PM.

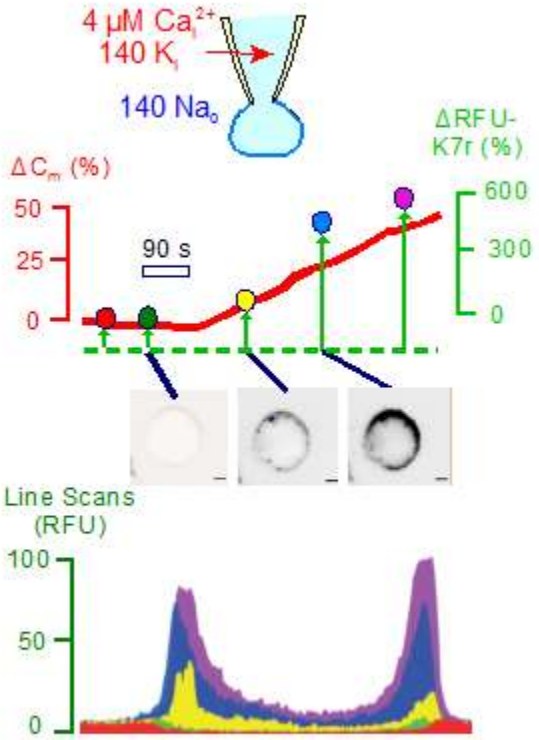

Figure 4. PM expansion and exposure of anionic phospholipids, as monitored by binding of heptalysine-rhodamine (K7r), follow similar time courses. A free cytoplasmic Ca^{2+} of 4 µM was maintained by employing highly Ca^{2+}-buffered cytoplasmic solutions. Similar to other membrane probes, K7r reveals the opening of deeply invaginating membrane compartments during PM expansion. Here and in all subsequent figures, concentrations are given in millimolar unless indicated otherwise.

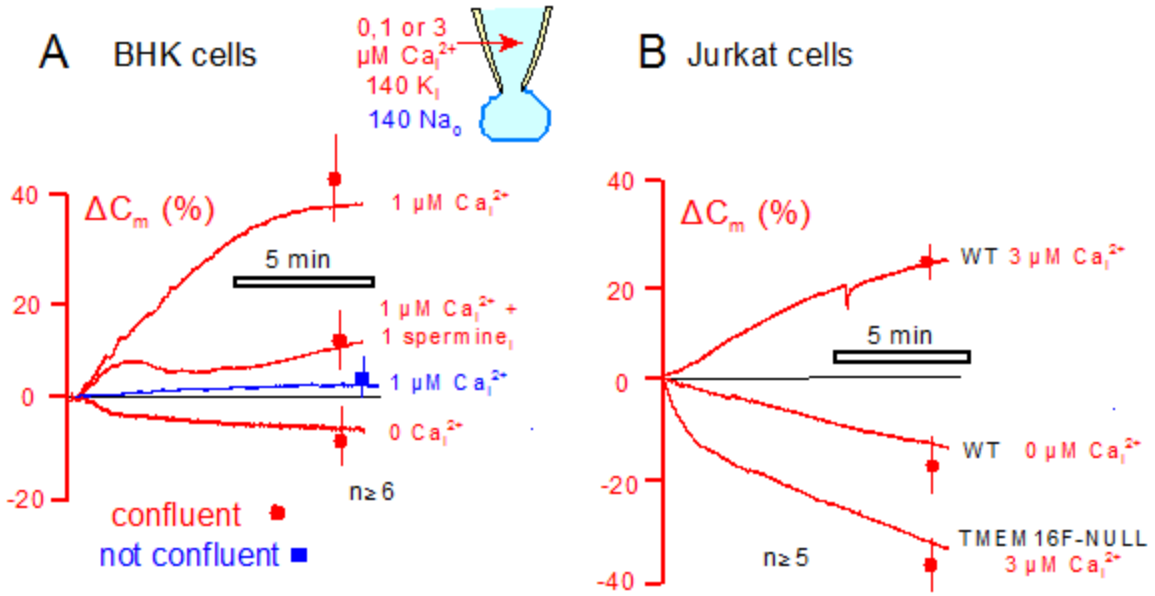

Figure 5. TMEM16F-mediated PM expansion can occur profusely with 1 to 3 μM free cytoplasmic Ca^{2+}, albeit slowly. **(A)** In BHK cells that were grown to just confluence (red records and error bars), membrane area (C_m) increases by 40% over 10 min when cells are perfused with solutions containing 1 μM free Ca^{2+}, buffered with 30 mM EGTA. PM expansion does not occur in the absence of Ca^{2+}, and PM expansion is blocked by spermine (1 mM), as expected from studies in Jurkat cells. BHK cells removed from dishes during their growth phase (i.e. subconfluent cells, blue record and error bars) exhibit no PM expansion during experiments with 1 μM free cytoplasmic Ca^{2+}. **(B)** In Jurkat cells, 3 μM free Ca^{2+} is required to elicit robust PM expansion that amounts to 25% of membrane area over 10 min. Membrane area decreases by 10% over 10 min in the absence of Ca^{2+}, and in TMEM16F-null cells membrane area decreases by 35% in the presence of 3 μM free Ca^{2+}.

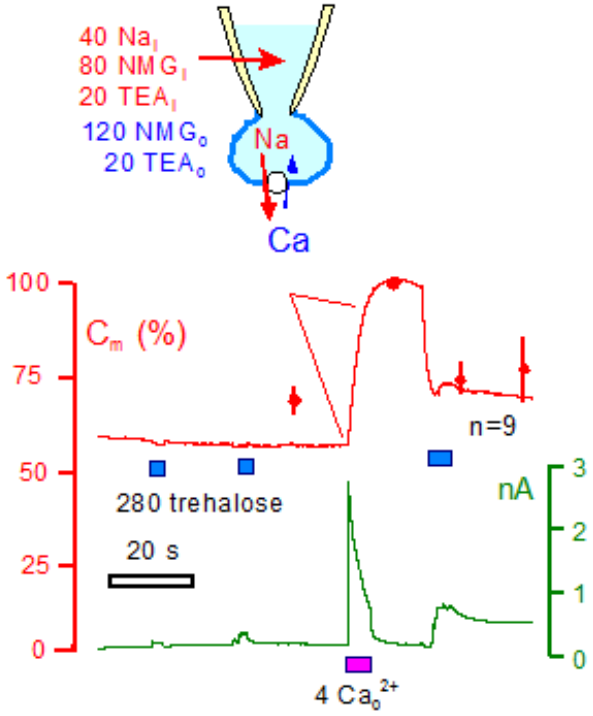

Figure 6. Reversal of PM expansion by replacement of extracellular ions with trehalose. Membrane compartments that expand the PM during Ca^{2+} influx in BHK cells can be closed by substitution of extracellular monovalent ions by trehalose. Ca^{2+} influx via reverse NCX activity results in a 75% increase of C_m on average in BHK cells (n=6) Application of trehalose within 30 s of the expansion response reverses the PM expansion by 86% on average.

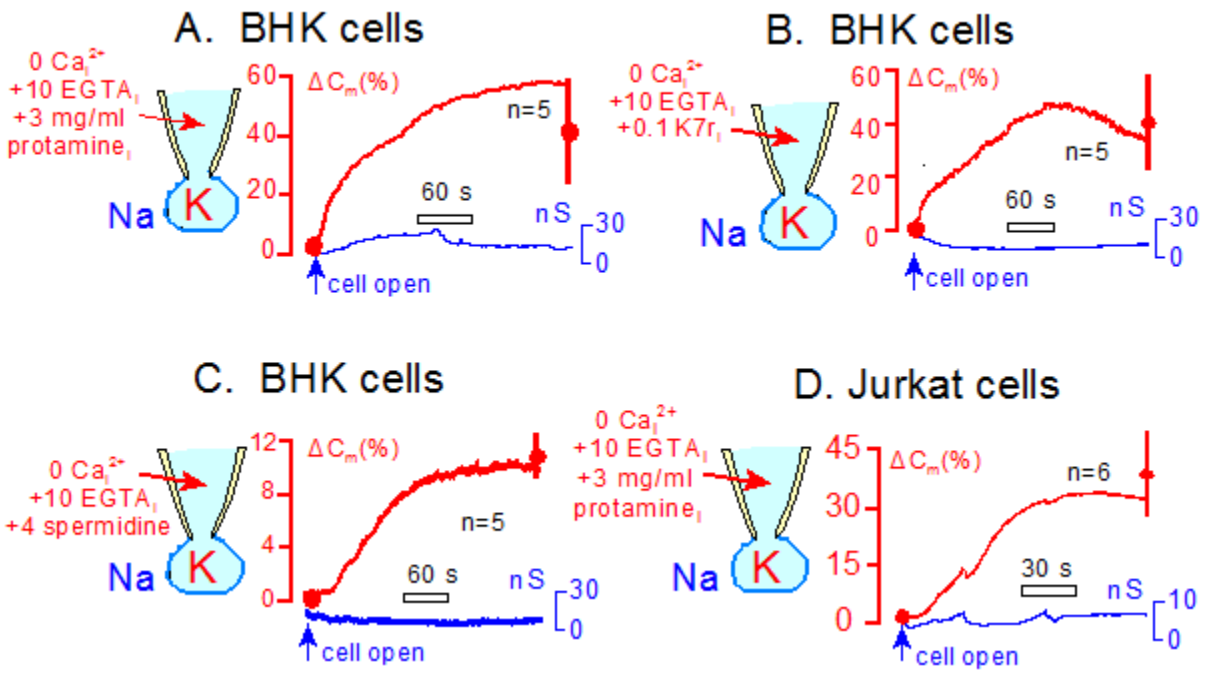

Figure 7. Peptides (heptalysine-rhodamine, K7r) and proteins (protamine) that bind anionic phospholipids cause PM expansion from the cytoplasmic side in the absence of Ca^{2+} (10 mM EGTA). (A) BHK cells increase membrane area by 29.7% on average when opened in the cytoplasmic presence of 3 mg/ml protamine. **(B)** BHK cells increase membrane area on average by 37.1 % when opened in the presence of 0.2 mM K7r. **(C)** Jurkat cells increase their membrane area by 40.1% on average when opened in the presence of 3 mg/ml protamine.

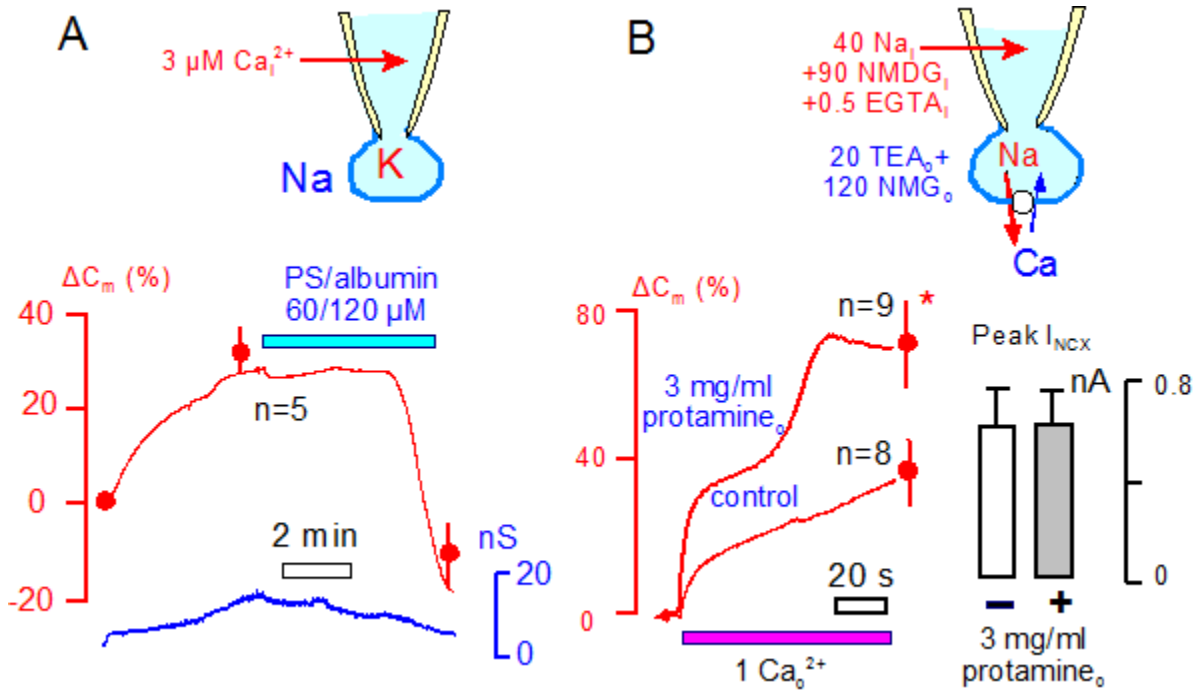

Figure 8. Reversal of PM expansion by extracellular PS-albumin complexes and enhancement of PM expansion by extracellular PS-binding peptides/proteins. (A) PM expansion in the presence of 3 μM free cytoplasmic Ca^{2+} can be reversed by application of extracellular PS-albumin complexes (120 μM). **(B)** PM expansion by reverse NCX activity in BHK cells can be doubled by including cationic proteins that bind PS (protamine, 3 mg/ml) in extracellular solutions. Activity of NCX is not affected by extracellular application of protamine.

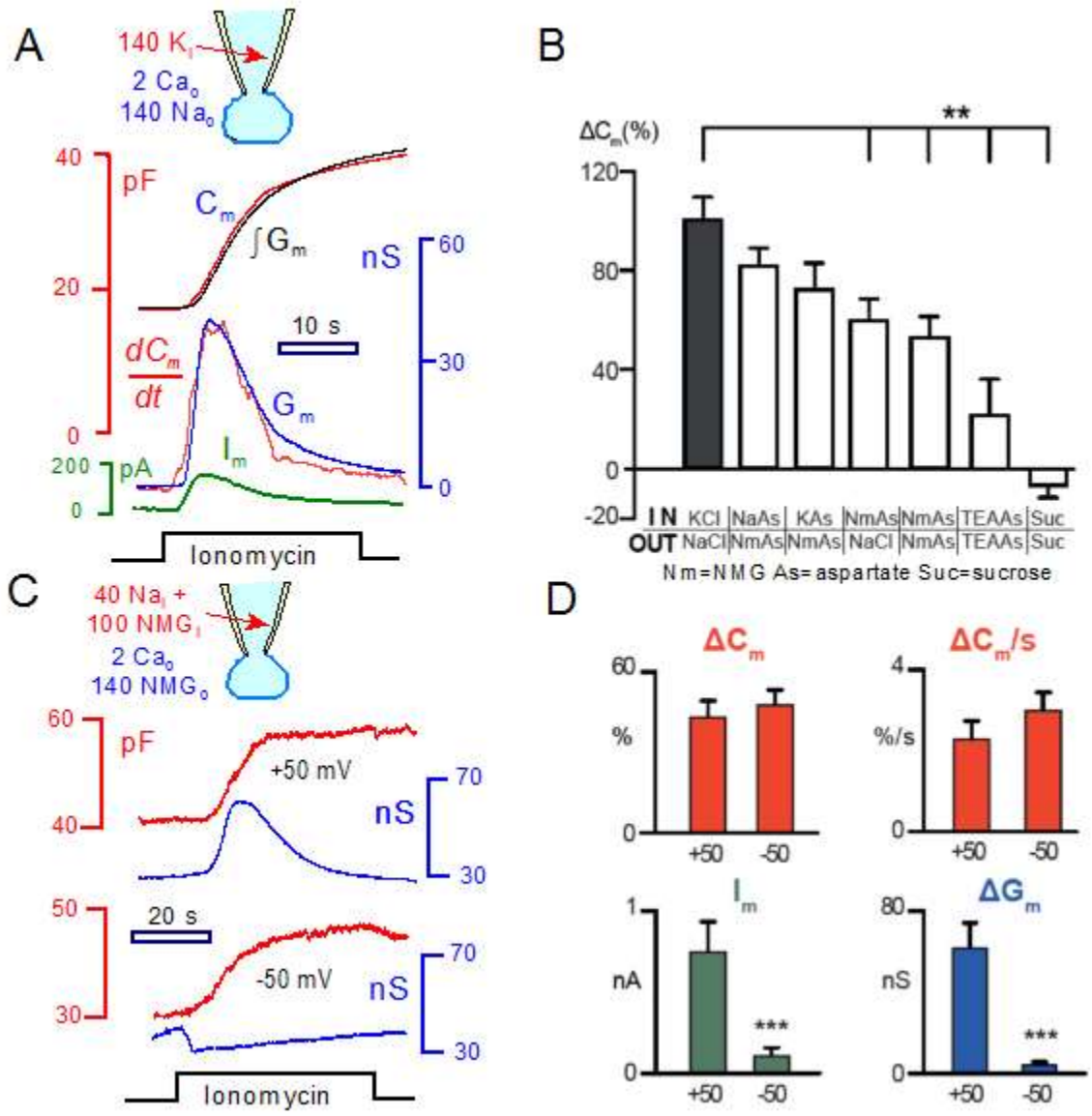

Figure 9. Relationships between membrane conductance (G_m), current (I_m) and capacitance (C_m) during ionomycin-induced PM expansion in Jurkat T cells. **(A)** Using standard experimental solutions with WT Jurkat T cells, G_m and I_m have similar time courses (lower recordings), and the integral of G_m, $\int G_m$, tracks the time course of PM expansion (ΔC_m) (upper recordings) during application of ionomycin (5 μM). Records were scaled to start and end at the same points, n >10. **(B)** Percentage change in C_m 30s after ionomycin treatment of WT Jurkat cells. Cells were perfused with indicated cytoplasmic solutions for >200s before ionomycin treatment. Extracellular (Out) and cytoplasmic (In) solutions were as shown: Standard cytoplasmic (KCl), Sodium Aspartate (NaAs), Potassium Aspartate (KAs), NMG Aspartate (NmAs), Ringer solution (NaCl), TEA and isotonic sucrose (Suc) with 0.5 mM EGTA

with 4 mM (Out) or 0.5 mM $MgCl_2$ (In). **(C and D)** Ion permeation does not influence PM expansion. Solutions were symmetrical NmAs with 30 mM NMG replaced by 30 mM Na on the cytoplasmic side to generate outward Na current. Membrane potential was held at +50 or – 50 mV during the entire experiments. Representative recordings are shown in **C**; mean values and SEM for n=7 at each potential are shown in **D.** Ionomycin treatment transiently increases conductance (blue) and generates outward Na current (green) at +50 mV but not at -50 mV. However, C_m (red) increases to the same extent and at the same maximal rate at -50 and +50 mV.

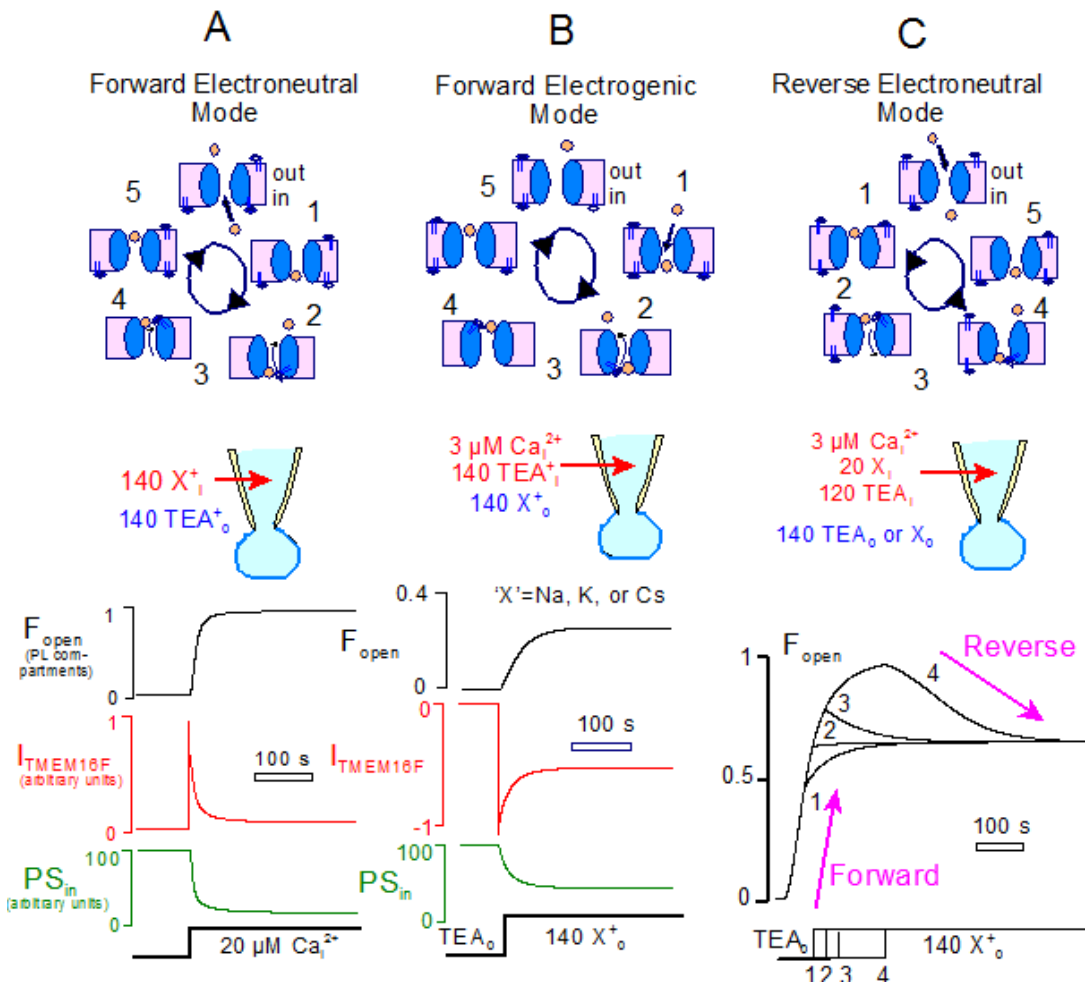

Figure 10. Simulation of TMEM16F function and PM expansion accompanying TMEM16F activation. (A) Predicted results for activation of TMEM16F by increasing cytoplasmic free Ca^{2+} from 0 to 20 μM (similar to reverse NCX activation or ionomycin exposure). Nearly all subsurface PM compartments open to the extracellular space, TMEM16F current inactivates by about 90%, and >80% of PS translocates from the cytoplasmic leaflet to the extracellular membrane leaflet. **(B)** PM expansion induced by applying 140 mM permeant cation on the extracellular side in the absence of permeant cations on the cytoplasmic side. PS translocates to the outside in an electrogenic fashion as a cation permeates inwardly and then retreats to the extracellular side with one PS molecule. **(C)** PM expansion induced by140 mM extracellular Cs when cytoplasmic solutions contain TEA and 20 mM Na. Responses 1 to 4 were generated by substituting extracellular Cs for TEA at progressively later time points. When PM expansion approaches steady state (4), PM expansion reverses by 30% when TEA is replaced by Cs in the extracellular solution.

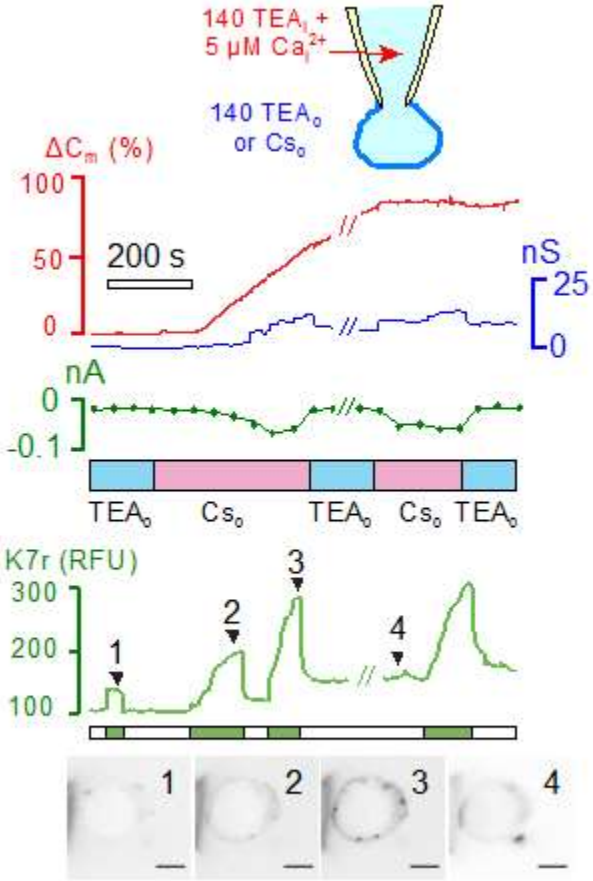

Figure 11. Activation of PM expansion and PS scrambling to the outer monolayer by extracellular Cs. The experiment was initiated with TEA on both membrane sides and with 5 μM Ca^{2+} on the cytoplasmic side. C_m is stable and K7r binding is initially very low. After 2.5 min, extracellular TEA was substituted for Cs, and PM expansion began within 1 min. K7r binding increases in parallel with PM expansion and remains reversible. Deep membrane compartments become labeled over time (see micrograph #3).

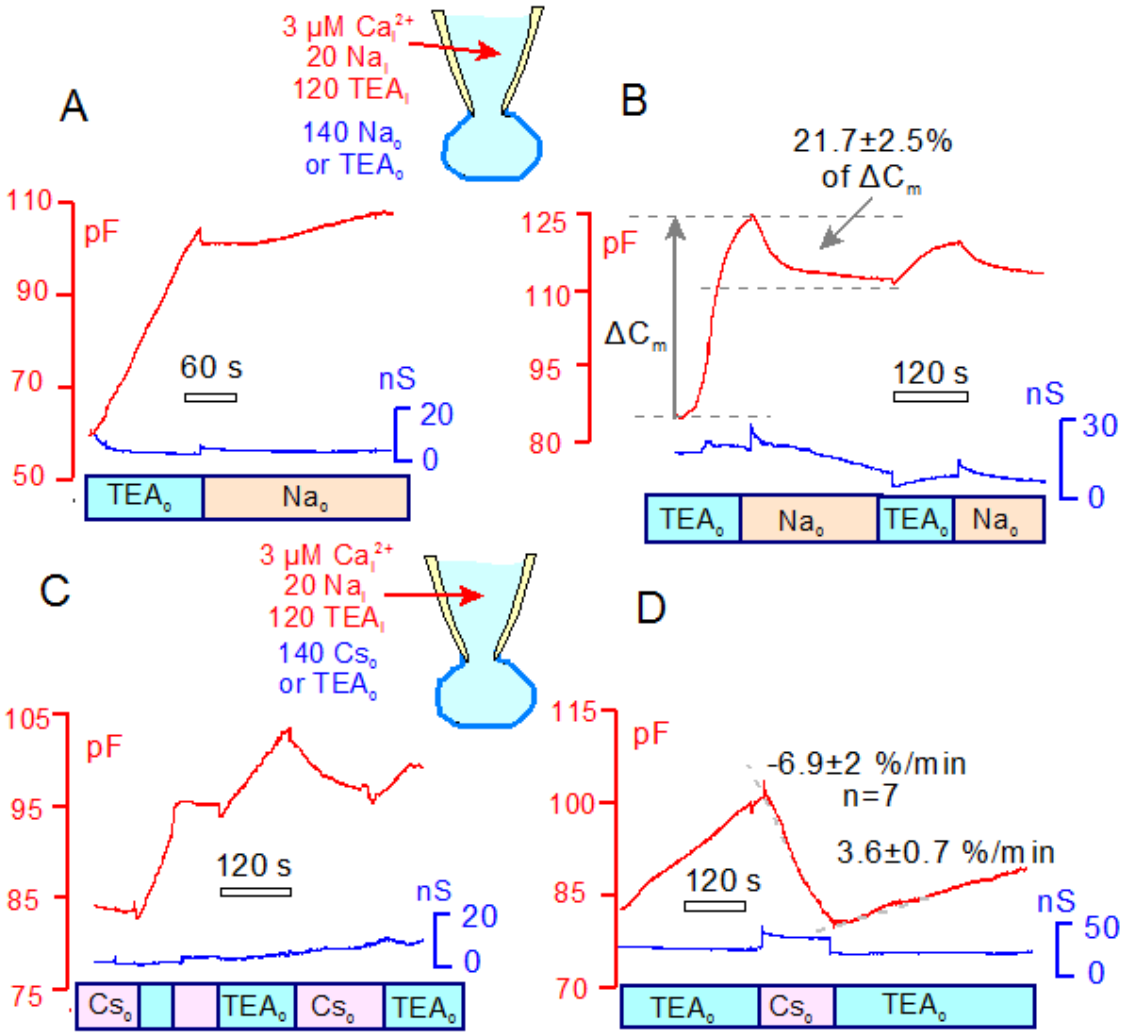

Figure 12. As predicted by simulations, whole-cell recordings reveal inhibition and reversal of PM expansion by extracellular Na and Cs in the presence of 20 mM cytoplasmic Na and 3 μM cytoplasmic free Ca^{2+}. **(A)** PM expansion proceed rapidly in the presence of extracellular TEA, and the expansion effectively stops when cytoplasmic TEA is substituted for Na. **(B)** After PM expansion reaches a near steady state in the presence of extracellular TEA, PM expansion reverses by 22% on average when extracellular TEA is substituted for Na. **(C)** Blockade and partial reversal of PM expansion by substituting extracellular TEA for Cs. **(D)** Reversal of PM expansion upon substituting extracellular TEA for Cs can occur with just a few seconds.

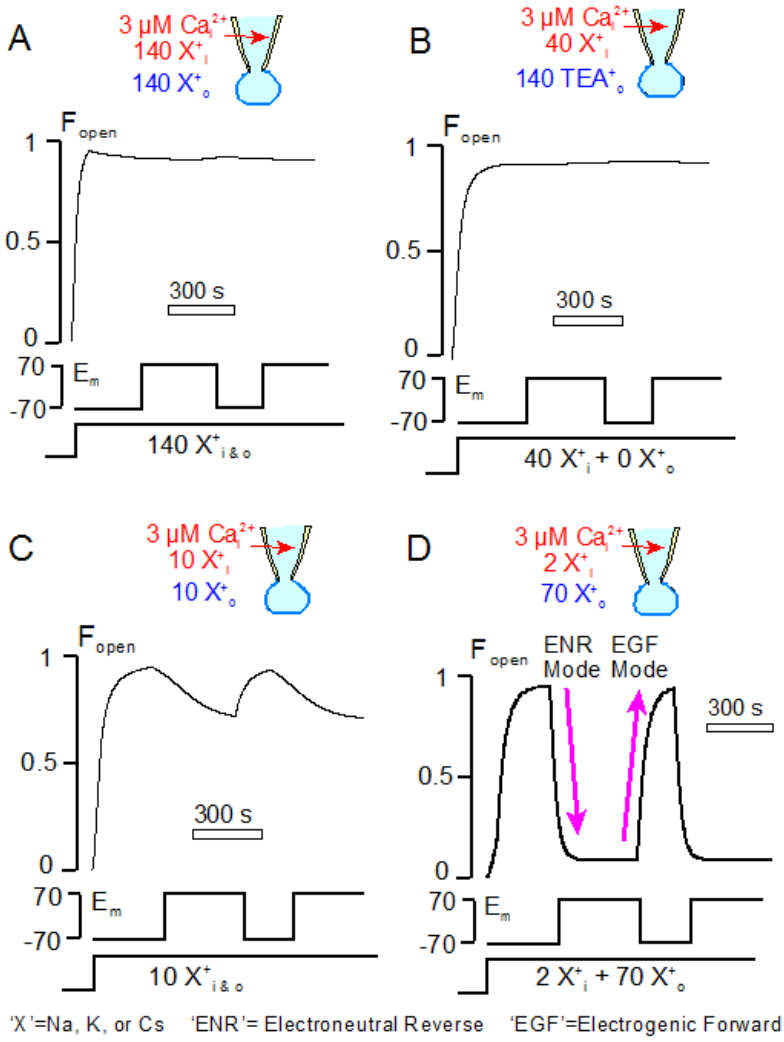

Figure 13. Simulation of effects of membrane potential on PM expansion during different modes of TMEM16F activity. The fraction of open invaginations (F_{open}) is simulated in the presence of 140 mM cytoplasmic TEA and either 140 mM TEA or Cs on the cytoplasmic side. The cytoplasmic solution is simulated to contain 3 μM free Ca^{2+}. **(A)** Extracellular TEA (140 mM) is substituted for Cs at 3 different membrane potentials (-70, 0 and +70 mV). Hyperpolarization promotes PM expansion, depolarization prevents PM expansion. **(B)** Depolarization reversibly causes closure of the deeply extended PM compartments, while hyperpolarization causes opening of the compartments under the condition of imposed inward cation gradients.

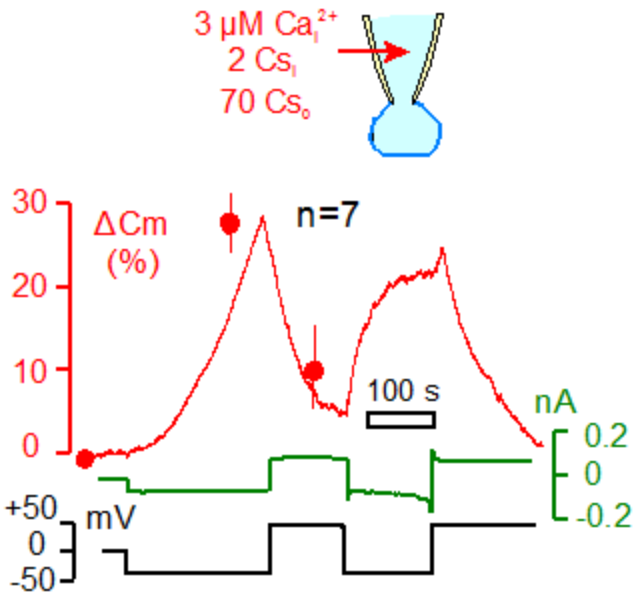

Figure 14. With an inward gradient of permeant monovalent cations PM expansion is promoted by hyperpolarization and reversed by depolarization. Verification of simulations in Fig. 13. The cytoplasmic solution contains no ATP, no Mg and no GTP. Using 2 mM cytoplasmic and 70 mM extracellular Cs in the presence of additionally 138 and 70 mM TEA, respectively, hyperpolarization drives extensive PM expansion that amounts to 30% over 4 min. Upon depolarization, PM expansion reverses, for the most part, and responses can be repeated. Hyperpolarization favors an electrogenic outward movement of PS under these conditions, while depolarization stops the electrogenic PS transport mode and thereby allows reverse PS transport from the outer to the inner monolayer.

Reference List

Anderson, R.G., B.A. Kamen, K.G. Rothberg, and S.W. Lacey. 1992. Potocytosis: sequestration and transport of small molecules by caveolae. *Science (New York, N.Y.)*. 255:410-411.

Antonny, B., C. Burd, P. De Camilli, E. Chen, O. Daumke, K. Faelber, M. Ford, V.A. Frolov, A. Frost, J.E. Hinshaw, T. Kirchhausen, M.M. Kozlov, M. Lenz, H.H. Low, H. McMahon, C. Merrifield, T.D. Pollard, P.J. Robinson, A. Roux, and S. Schmid. 2016. Membrane fission by dynamin: what we know and what we need to know. *The EMBO journal*. 35:2270-2284. doi:10.15252/embj.201694613.

Bartholow, L.C., and R.P. Geyer. 1982. Influence of phospholipid structure on sterol efflux induced by albumin-phospholipid complexes. *Biochemistry*. 21:1271-1273.

Bradke, F., J.W. Fawcett, and M.E. Spira. 2012. Assembly of a new growth cone after axotomy: the precursor to axon regeneration. *Nature reviews. Neuroscience*. 13:183-193. doi:10.1038/nrn3176.

Bretscher, M.S. 2008. Exocytosis provides the membrane for protrusion, at least in migrating fibroblasts. *Nature reviews. Molecular cell biology*. 9:916. doi:10.1038/nrm2419-c3.

Bricogne, C.e.a. XXXX. TMEM16F activation by Ca2+ triggers surface membrane expansion and directs Programmed Death receptor (PD-1) trafficking. . *eLife*. xx:xxx-xxx.

Carr, J.A., and N. Silverman. 1999. The heparin-protamine interaction. A review. *The Journal of cardiovascular surgery*. 40:659-666.

Cocucci, E., G. Racchetti, P. Podini, and J. Meldolesi. 2007. Enlargeosome traffic: exocytosis triggered by various signals is followed by endocytosis, membrane shedding or both. *Traffic (Copenhagen, Denmark)*. 8:742-757. doi:10.1111/j.1600-0854.2007.00566.x.

Cocucci, E., G. Racchetti, M. Rupnik, and J. Meldolesi. 2008. The regulated exocytosis of enlargeosomes is mediated by a SNARE machinery that includes VAMP4. *Journal of cell science*. 121:2983-2991. doi:10.1242/jcs.032029.

Cohen, R., B.M. Schmitt, and D. Atlas. 2008. Reconstitution of depolarization and Ca2+-evoked secretion in Xenopus oocytes monitored by membrane capacitance. *Methods in molecular biology (Clifton, N.J.)*. 440:269-282. doi:10.1007/978-1-59745-178-9_21.

Cooper, S.T., and P.L. McNeil. 2015. Membrane Repair: Mechanisms and Pathophysiology. *Physiological reviews*. 95:1205-1240. doi:10.1152/physrev.00037.2014.

Coorssen, J.R., H. Schmitt, and W. Almers. 1996. Ca2+ triggers massive exocytosis in Chinese hamster ovary cells. *The EMBO journal*. 15:3787-3791.

Corrotte, M., T. Castro-Gomes, A.B. Koushik, and N.W. Andrews. 2015. Approaches for plasma membrane wounding and assessment of lysosome-mediated repair responses. *Methods in cell biology*. 126:139-158. doi:10.1016/bs.mcb.2014.11.009.

Cribier, S., G. Morrot, J.M. Neumann, and P.F. Devaux. 1990. Lateral diffusion of erythrocyte phospholipids in model membranes comparison between inner and outer leaflet components. *European biophysics journal : EBJ*. 18:33-41.

Demonbreun, A.R., and E.M. McNally. 2016. Plasma Membrane Repair in Health and Disease. *Current topics in membranes*. 77:67-96. doi:10.1016/bs.ctm.2015.10.006.

Denisov, G., S. Wanaski, P. Luan, M. Glaser, and S. McLaughlin. 1998. Binding of basic peptides to membranes produces lateral domains enriched in the acidic lipids phosphatidylserine

and phosphatidylinositol 4,5-bisphosphate: an electrostatic model and experimental results. *Biophysical journal*. 74:731-744. doi:10.1016/s0006-3495(98)73998-0.

Fujii, T., A. Sakata, S. Nishimura, K. Eto, and S. Nagata. 2015. TMEM16F is required for phosphatidylserine exposure and microparticle release in activated mouse platelets. *Proceedings of the National Academy of Sciences of the United States of America*. 112:12800-12805. doi:10.1073/pnas.1516594112.

Fulop, T., S. Radabaugh, and C. Smith. 2005. Activity-dependent differential transmitter release in mouse adrenal chromaffin cells. *The Journal of neuroscience : the official journal of the Society for Neuroscience*. 25:7324-7332. doi:10.1523/jneurosci.2042-05.2005.

Gadella, B.M., and J.P. Evans. 2011. Membrane fusions during mammalian fertilization. *Advances in experimental medicine and biology*. 713:65-80. doi:10.1007/978-94-007-0763-4_5.

Groulx, N., F. Boudreault, S.N. Orlov, and R. Grygorczyk. 2006. Membrane reserves and hypotonic cell swelling. *The Journal of membrane biology*. 214:43-56. doi:10.1007/s00232-006-0080-8.

Harrisson, F., M. Callebaut, and L. Vakaet. 1981. Microspectrographic analysis of trypan blue-induced fluorescence in oocytes of the Japanese quail. *Histochemistry*. 72:563-578.

Hilgemann, D.W., G. Dai, A. Collins, V. Lariccia, S. Magi, C. Deisl, and M. Fine. 2018. Lipid signaling to membrane proteins: From second messengers to membrane domains and adapter-free endocytosis. *The Journal of general physiology*. doi:10.1085/jgp.201711875.

Hilgemann, D.W., and M. Fine. 2011. Mechanistic analysis of massive endocytosis in relation to functionally defined surface membrane domains. *The Journal of general physiology*. 137:155-172. doi:10.1085/jgp.201010470.

Hirama, T., R. Das, Y. Yang, C. Ferguson, A. Won, C.M. Yip, J.G. Kay, S. Grinstein, R.G. Parton, and G.D. Fairn. 2017. Phosphatidylserine dictates the assembly and dynamics of caveolae in the plasma membrane. *The Journal of biological chemistry*. 292:14292-14307. doi:10.1074/jbc.M117.791400.

Ichev, K., W. Ovtscharoff, U. Pfuller, P. Bergmann, H. Franz, and L. Venkov. 1985. Distribution of negative charges of rat brain synaptosomes established by means of protamine-ferritin conjugate. *Acta histochemica*. 77:117-120. doi:10.1016/s0065-1281(85)80023-4.

Kapla, J., J. Wohlert, B. Stevensson, O. Engstrom, G. Widmalm, and A. Maliniak. 2013. Molecular dynamics simulations of membrane-sugar interactions. *The journal of physical chemistry. B*. 117:6667-6673. doi:10.1021/jp402385d.

Kasai, H., T. Kishimoto, T.T. Liu, Y. Miyashita, P. Podini, F. Grohovaz, and J. Meldolesi. 1999. Multiple and diverse forms of regulated exocytosis in wild-type and defective PC12 cells. *Proceedings of the National Academy of Sciences of the United States of America*. 96:945-949.

Kreft, M., M. Stenovec, M. Rupnik, S. Grilc, M. Krzan, M. Potokar, T. Pangrsic, P.G. Haydon, and R. Zorec. 2004. Properties of Ca(2+)-dependent exocytosis in cultured astrocytes. *Glia*. 46:437-445. doi:10.1002/glia.20018.

Lam, C.F., and D.G. Priest. 1972. Enzyme kinetics. Systematic generation of valid King-Altman patterns. *Biophysical journal*. 12:248-256. doi:10.1016/s0006-3495(72)86084-3.

Lariccia, V., M. Fine, S. Magi, M.J. Lin, A. Yaradanakul, M.C. Llaguno, and D.W. Hilgemann. 2011. Massive calcium-activated endocytosis without involvement of classical endocytic proteins. *The Journal of general physiology*. 137:111-132. doi:10.1085/jgp.201010468.

Lewis, S.A., and J.L. de Moura. 1984. Apical membrane area of rabbit urinary bladder increases by fusion of intracellular vesicles: an electrophysiological study. *The Journal of membrane biology*. 82:123-136.

McMahon, H.T., and E. Boucrot. 2015. Membrane curvature at a glance. *Journal of cell science*. 128:1065-1070. doi:10.1242/jcs.114454.

Moe, A.M., A.E. Golding, and W.M. Bement. 2015. Cell healing: Calcium, repair and regeneration. *Seminars in cell & developmental biology*. 45:18-23. doi:10.1016/j.semcdb.2015.09.026.

Ninomiya, Y., T. Kishimoto, Y. Miyashita, and H. Kasai. 1996. Ca2+-dependent exocytotic pathways in Chinese hamster ovary fibroblasts revealed by a caged-Ca2+ compound. *The Journal of biological chemistry*. 271:17751-17754.

Racchetti, G., R. D'Alessandro, and J. Meldolesi. 2012. Astrocyte stellation, a process dependent on Rac1 is sustained by the regulated exocytosis of enlargeosomes. *Glia*. 60:465-475. doi:10.1002/glia.22280.

Salzer, U., J. Kostan, and K. Djinovic-Carugo. 2017. Deciphering the BAR code of membrane modulators. *Cellular and molecular life sciences : CMLS*. 74:2413-2438. doi:10.1007/s00018-017-2478-0.

Schmid, S.L., M.A. McNiven, and P. De Camilli. 1998. Dynamin and its partners: a progress report. *Current opinion in cell biology*. 10:504-512.

Scudieri, P., E. Caci, A. Venturini, E. Sondo, G. Pianigiani, C. Marchetti, R. Ravazzolo, F. Pagani, and L.J. Galietta. 2015. Ion channel and lipid scramblase activity associated with expression of TMEM16F/ANO6 isoforms. *The Journal of physiology*. 593:3829-3848. doi:10.1113/jp270691.

Shaul, P.W., and R.G. Anderson. 1998. Role of plasmalemmal caveolae in signal transduction. *The American journal of physiology*. 275:L843-851.

Stevens, C.F., and J.H. Williams. 2000. "Kiss and run" exocytosis at hippocampal synapses. *Proceedings of the National Academy of Sciences of the United States of America*. 97:12828-12833. doi:10.1073/pnas.230438697.

Sudhof, T.C. 2012. Calcium control of neurotransmitter release. *Cold Spring Harbor perspectives in biology*. 4:a011353. doi:10.1101/cshperspect.a011353.

Sudhof, T.C., and J.E. Rothman. 2009. Membrane fusion: grappling with SNARE and SM proteins. *Science (New York, N.Y.)*. 323:474-477. doi:10.1126/science.1161748.

Suetsugu, S. 2016. Higher-order assemblies of BAR domain proteins for shaping membranes. *Microscopy (Oxford, England)*. 65:201-210. doi:10.1093/jmicro/dfw002.

Suzuki, J., T. Fujii, T. Imao, K. Ishihara, H. Kuba, and S. Nagata. 2013. Calcium-dependent phospholipid scramblase activity of TMEM16 protein family members. *The Journal of biological chemistry*. 288:13305-13316. doi:10.1074/jbc.M113.457937.

Togo, T., J.M. Alderton, G.Q. Bi, and R.A. Steinhardt. 1999. The mechanism of facilitated cell membrane resealing. *Journal of cell science*. 112 (Pt 5):719-731.

Togo, T., J.M. Alderton, and R.A. Steinhardt. 2003. Long-term potentiation of exocytosis and cell membrane repair in fibroblasts. *Molecular biology of the cell*. 14:93-106. doi:10.1091/mbc.E02-01-0056.

Tojima, T., R. Itofusa, and H. Kamiguchi. 2014. Steering neuronal growth cones by shifting the imbalance between exocytosis and endocytosis. *The Journal of neuroscience : the official journal of the Society for Neuroscience*. 34:7165-7178. doi:10.1523/jneurosci.5261-13.2014.

van den Bogaart, G., N. Hermans, V. Krasnikov, A.H. de Vries, and B. Poolman. 2007. On the decrease in lateral mobility of phospholipids by sugars. *Biophysical journal*. 92:1598-1605. doi:10.1529/biophysj.106.096461.

Wang, T.M., and D.W. Hilgemann. 2008. Ca-dependent nonsecretory vesicle fusion in a secretory cell. *The Journal of general physiology*. 132:51-65. doi:10.1085/jgp.200709950.

Yang, H., A. Kim, T. David, D. Palmer, T. Jin, J. Tien, F. Huang, T. Cheng, S.R. Coughlin, Y.N. Jan, and L.Y. Jan. 2012. TMEM16F forms a Ca2+-activated cation channel required for lipid scrambling in platelets during blood coagulation. *Cell*. 151:111-122. doi:10.1016/j.cell.2012.07.036.

Yaradanakul, A., T.M. Wang, V. Lariccia, M.J. Lin, C. Shen, X. Liu, and D.W. Hilgemann. 2008. Massive Ca-induced membrane fusion and phospholipid changes triggered by reverse Na/Ca exchange in BHK fibroblasts. *The Journal of general physiology*. 132:29-50. doi:10.1085/jgp.200709865.

Figure 1

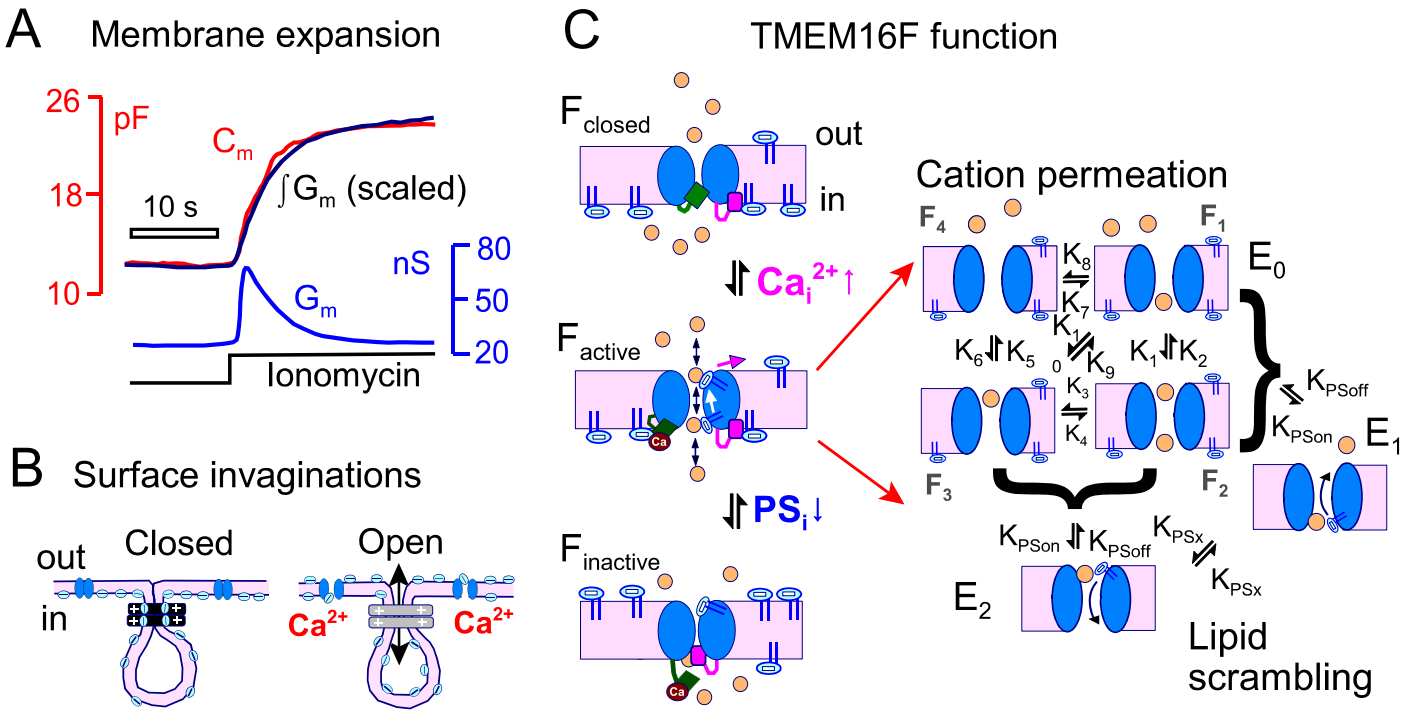
A
Membrane expansion
26
pF
18
10
10 s
Cm
∫Gm (scaled)
nS
80
50
20
Gm
Ionomycin
B
Surface invaginations
out
in
Closed
Open
Ca2+
Ca2+
C
TMEM16F function
Fclosed
out
in
Cai2+↑
Factive
PSi↓
Finactive
Cation permeation
F4
F1
E0
K8
K7
K1
K6
K5
0
K9
K1
K2
K3
K4
KPSoff
KPSon
E1
F3
F2
KPSon
KPSoff
KPSx
KPSx
E2
Lipid
scrambling

Figure 2

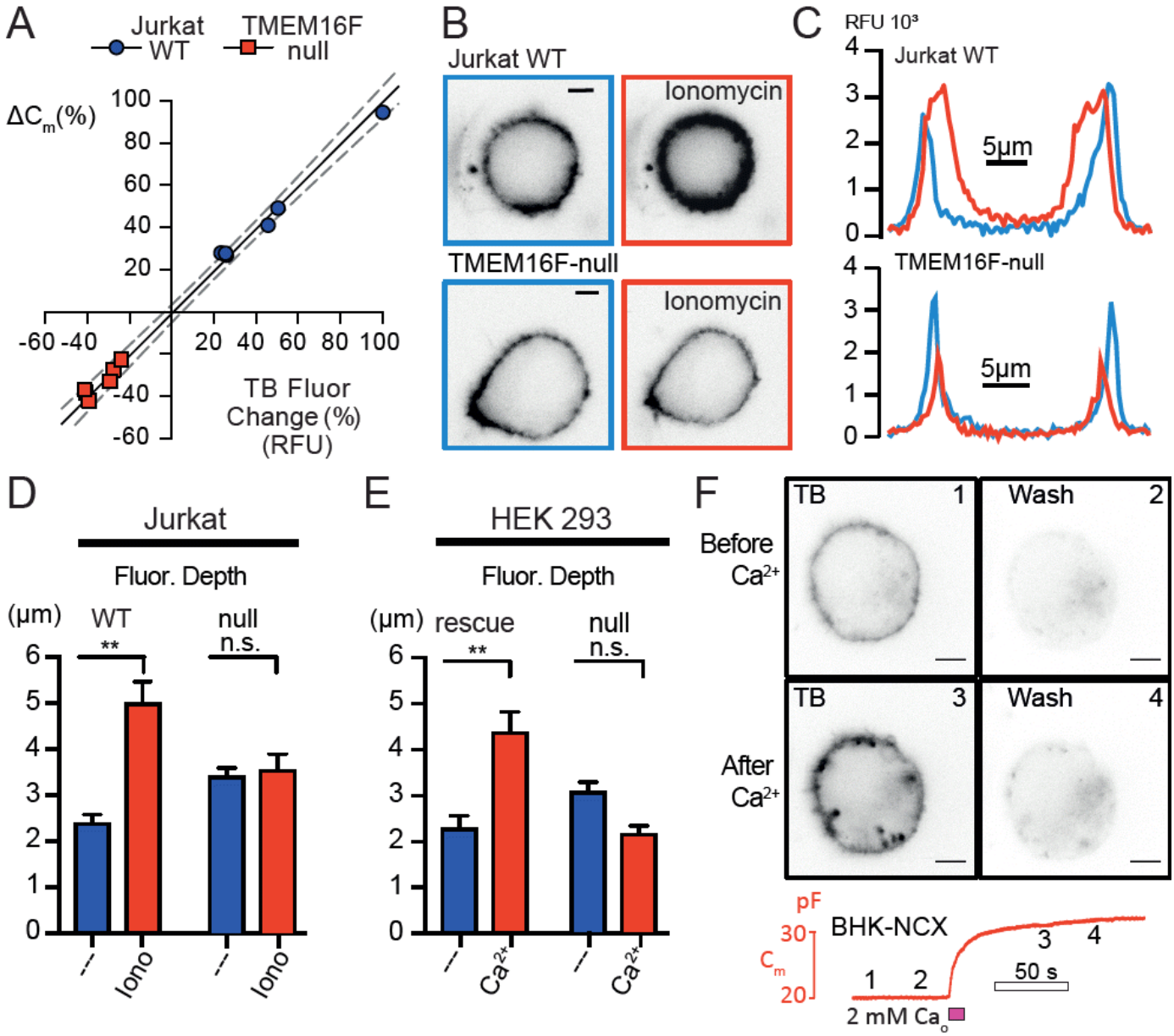
A
Jurkat WT
TMEM16F null
ΔCm(%)
100
80
60
40
20
-60 -40
20 40 60 80 100
-40
-60
TB Fluor Change (%) (RFU)
B
Jurkat WT
Ionomycin
TMEM16F-null
Ionomycin
C
RFU 10³
Jurkat WT
5μm
TMEM16F-null
5μm
D
Jurkat
Fluor. Depth
(μm)
WT
null
n.s.
**
--
Iono
E
HEK 293
Fluor. Depth
(μm)
rescue
null
n.s.
**
--
Ca2+
F
Before Ca2+
After Ca2+
TB 1
Wash 2
TB 3
Wash 4
pF
30
20
Cm
BHK-NCX
1 2 3 4
50 s
2 mM Cao

Figure 3

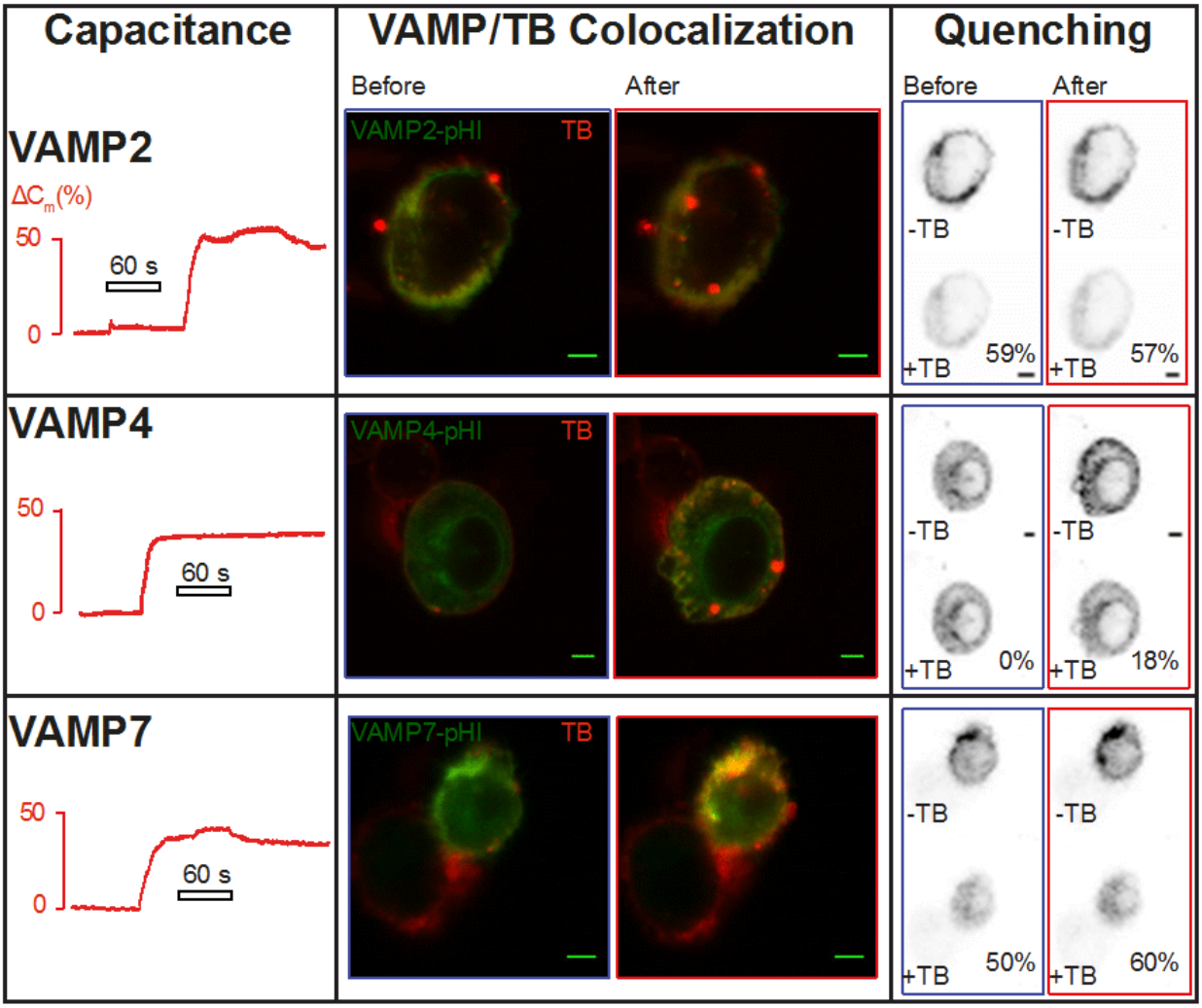
Capacitance
VAMP/TB Colocalization
Quenching
Before
After
Before
After
VAMP2
ΔCm(%)
50
0
60 s
VAMP2-pHI
TB
-TB
+TB
59%
57%
VAMP4
50
0
60 s
VAMP4-pHI
TB
-TB
+TB
0%
18%
VAMP7
50
0
60 s
VAMP7-pHI
TB
-TB
+TB
50%
60%

Figure 4

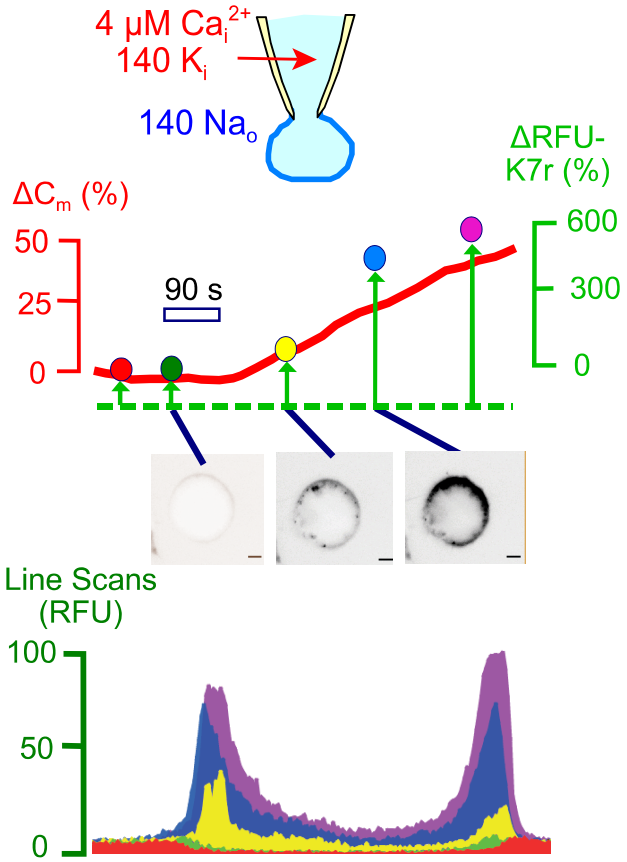
4 μM Ca_i^{2+}
140 K_i
140 Na_o
ΔRFU-
K7r (%)
$ΔC_m$ (%)
50
25
0
90 s
600
300
0
Line Scans
(RFU)
100
50
0

Figure 5

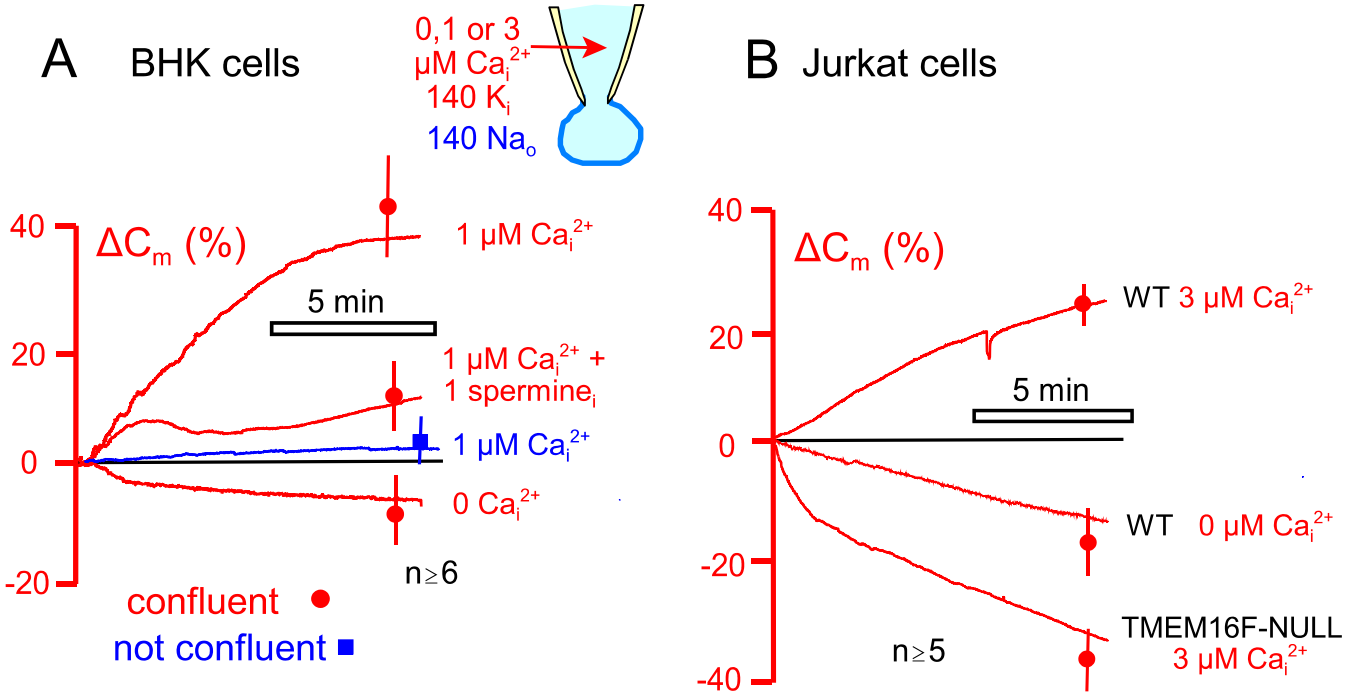
A
BHK cells
0,1 or 3
μM Ca$_i^{2+}$
140 K$_i$
140 Na$_o$
40
20
0
-20
ΔC$_m$ (%)
1 μM Ca$_i^{2+}$
5 min
1 μM Ca$_i^{2+}$ +
1 spermine$_i$
1 μM Ca$_i^{2+}$
0 Ca$_i^{2+}$
n≥6
confluent
not confluent
B
Jurkat cells
40
20
0
-20
-40
ΔC$_m$ (%)
WT 3 μM Ca$_i^{2+}$
5 min
WT 0 μM Ca$_i^{2+}$
TMEM16F-NULL
3 μM Ca$_i^{2+}$
n≥5

Figure 6

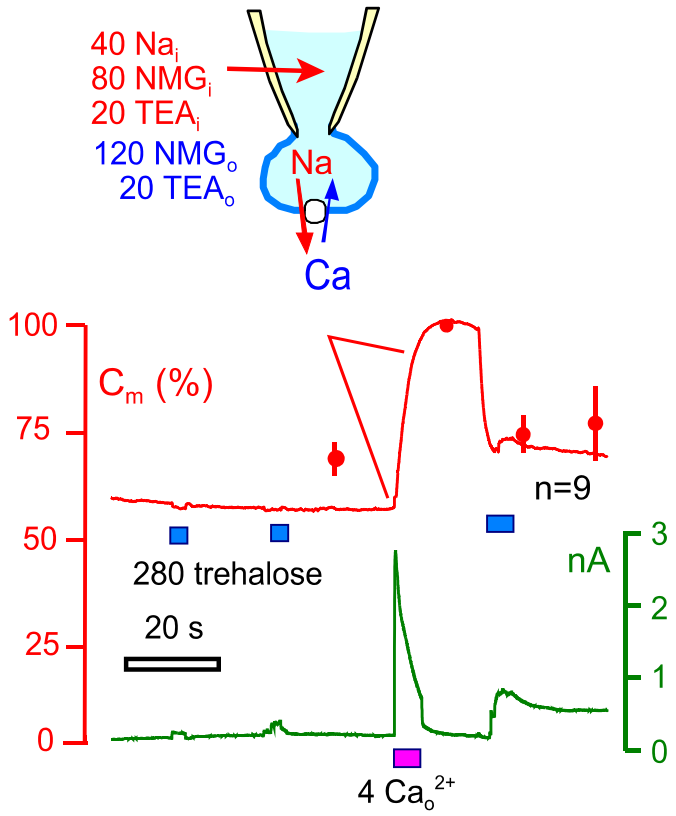
40 Na$_i$
80 NMG$_i$
20 TEA$_i$
120 NMG$_o$
20 TEA$_o$
Na
Ca
100
75
50
25
0
C$_m$ (%)
n=9
280 trehalose
20 s
nA
3
2
1
0
4 Ca$_o^{2+}$

Figure 7

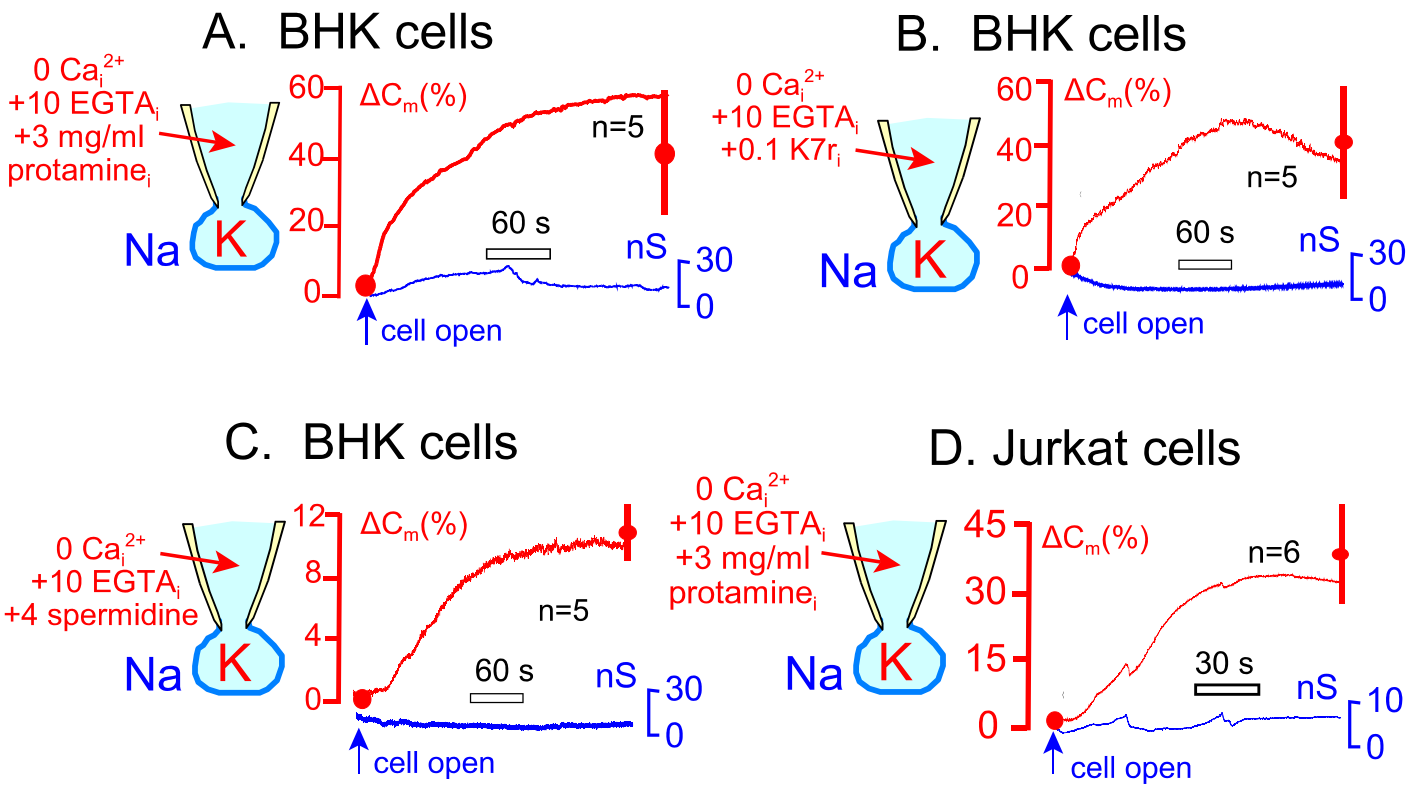
A. BHK cells
0 Ca$_i^{2+}$
+10 EGTA$_i$
+3 mg/ml
protamine$_i$
Na
K
60
40
20
0
ΔC$_m$(%)
n=5
60 s
nS
30
0
cell open
B. BHK cells
0 Ca$_i^{2+}$
+10 EGTA$_i$
+0.1 K7r$_i$
Na
K
60
40
20
0
ΔC$_m$(%)
n=5
60 s
nS
30
0
cell open
C. BHK cells
0 Ca$_i^{2+}$
+10 EGTA$_i$
+4 spermidine
Na
K
12
8
4
0
ΔC$_m$(%)
n=5
60 s
nS
30
0
cell open
D. Jurkat cells
0 Ca$_i^{2+}$
+10 EGTA$_i$
+3 mg/ml
protamine$_i$
Na
K
45
30
15
0
ΔC$_m$(%)
n=6
30 s
nS
10
0
cell open

Figure 8

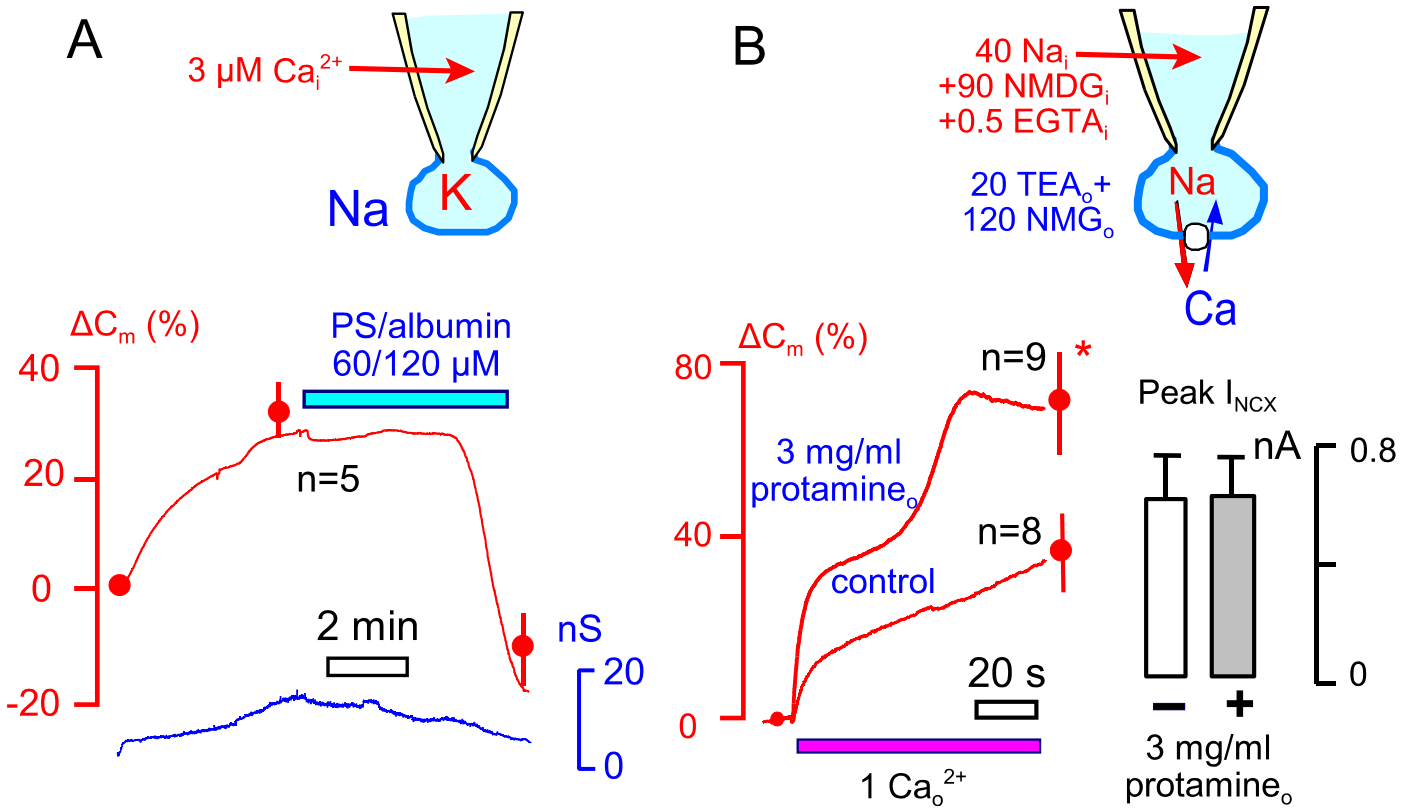
A
3 μM Ca$_i^{2+}$
Na
K
ΔC$_m$ (%)
PS/albumin
60/120 μM
40
20
0
-20
n=5
2 min
nS
20
0
B
40 Na$_i$
+90 NMDG$_i$
+0.5 EGTA$_i$
20 TEA$_o$+
120 NMG$_o$
Na
Ca
ΔC$_m$ (%)
80
40
0
n=9
*
3 mg/ml
protamine$_o$
n=8
control
20 s
1 Ca$_o^{2+}$
Peak I$_{NCX}$
nA
0.8
0
−
+
3 mg/ml
protamine$_o$

Figure 9

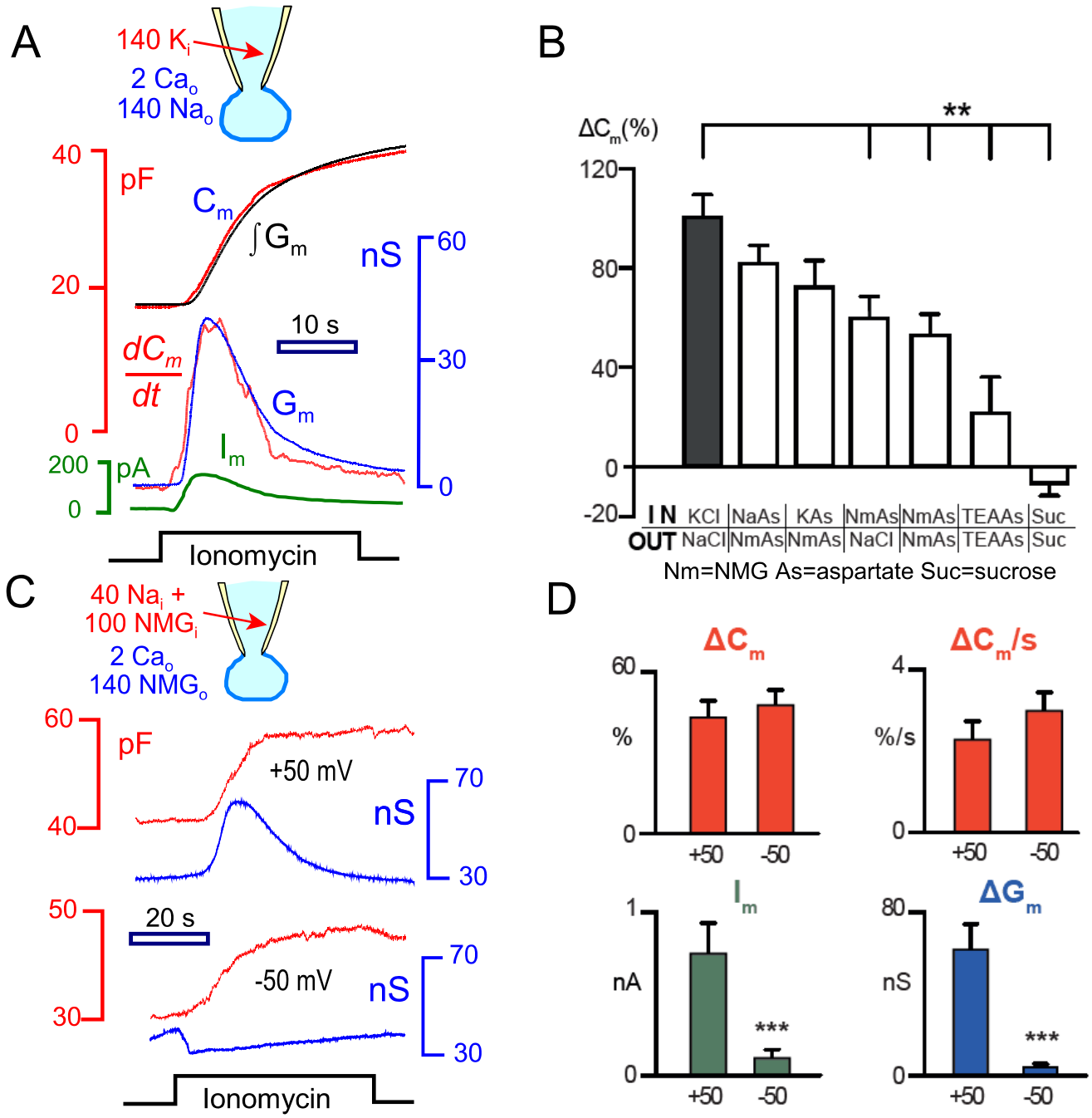
A
140 Ki
2 Cao
140 Nao
40
pF
20
0
Cm
∫Gm
nS
60
30
0
10 s
dCm/dt
Gm
Im
200
pA
0
Ionomycin
B
ΔCm(%)
**
120
80
40
0
-20
IN KCl NaAs KAs NmAs NmAs TEAAs Suc
OUT NaCl NmAs NmAs NaCl NmAs TEAAs Suc
Nm=NMG As=aspartate Suc=sucrose
C
40 Nai +
100 NMGi
2 Cao
140 NMGo
60
pF
40
+50 mV
nS
70
30
50
20 s
30
-50 mV
nS
70
30
Ionomycin
D
ΔCm
60
%
0
+50
-50
ΔCm/s
4
%/s
0
+50
-50
Im
1
nA
***
0
+50
-50
ΔGm
80
nS
***
0
+50
-50

Figure 10

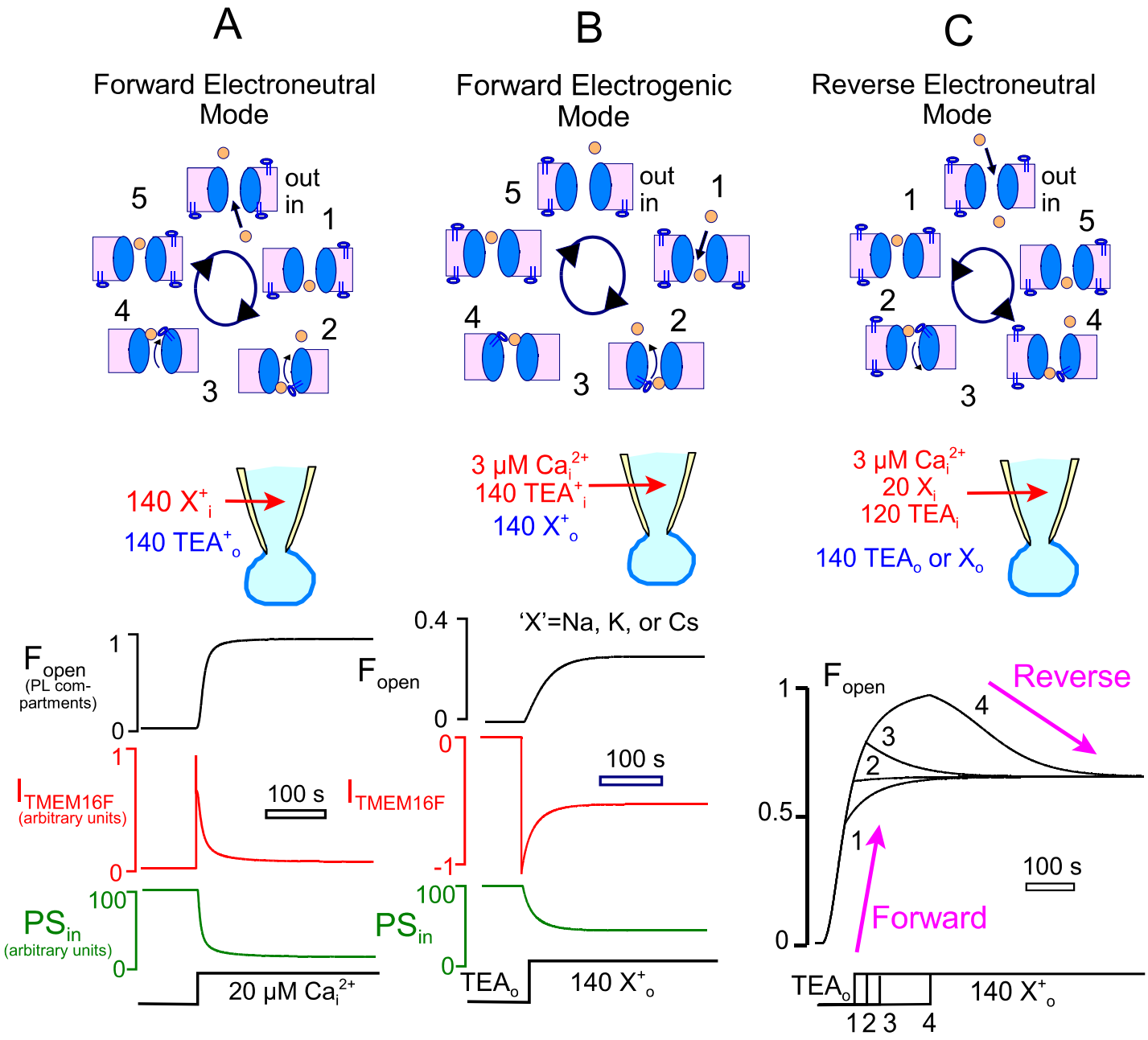
A
Forward Electroneutral Mode
B
Forward Electrogenic Mode
C
Reverse Electroneutral Mode
out
in
140 X+i
140 TEA+o
3 μM Cai2+
140 TEA+i
140 X+o
3 μM Cai2+
20 Xi
120 TEAi
140 TEAo or Xo
Fopen (PL com-partments)
ITMEM16F (arbitrary units)
PSin (arbitrary units)
100 s
20 μM Cai2+
'X'=Na, K, or Cs
Fopen
ITMEM16F
PSin
TEAo
140 X+o
Reverse
Forward
1 2 3 4

Figure 11

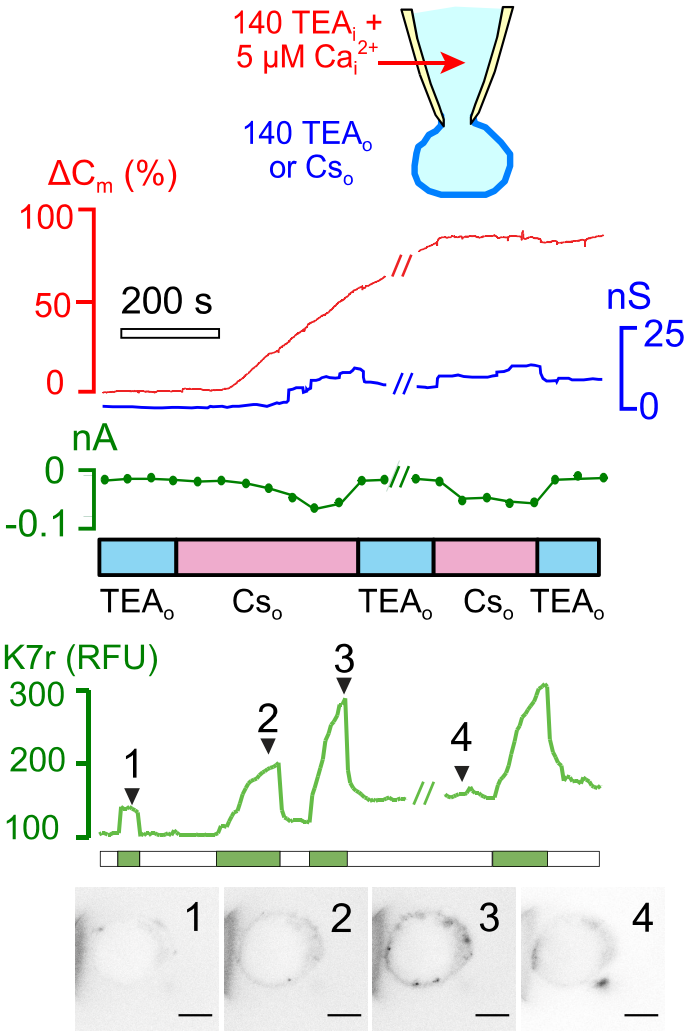
140 TEA$_i$ +
5 µM Ca$_i^{2+}$
140 TEA$_o$
or Cs$_o$
ΔC$_m$ (%)
100
50
0
200 s
nS
25
0
nA
0
-0.1
TEA$_o$
Cs$_o$
TEA$_o$
Cs$_o$
TEA$_o$
K7r (RFU)
300
200
100
1
2
3
4

Figure 12

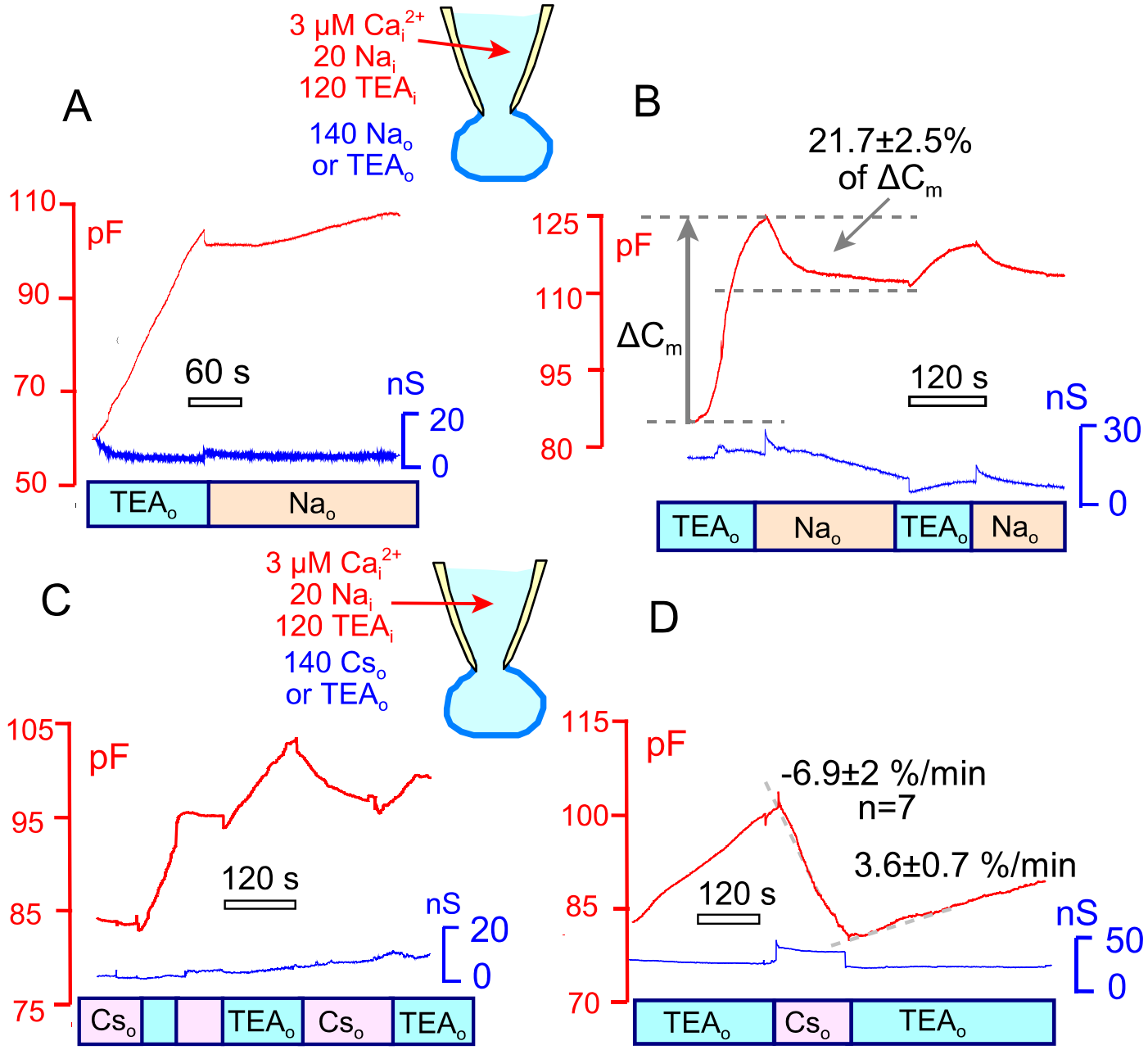
A
3 μM Ca$_i^{2+}$
20 Na$_i$
120 TEA$_i$
140 Na$_o$
or TEA$_o$
110
90
70
50
pF
60 s
nS
20
0
TEA$_o$
Na$_o$
B
21.7±2.5%
of ΔC$_m$
125
110
95
80
pF
ΔC$_m$
120 s
nS
30
0
TEA$_o$
Na$_o$
TEA$_o$
Na$_o$
C
3 μM Ca$_i^{2+}$
20 Na$_i$
120 TEA$_i$
140 Cs$_o$
or TEA$_o$
105
95
85
75
pF
120 s
nS
20
0
Cs$_o$
TEA$_o$
Cs$_o$
TEA$_o$
D
115
100
85
70
pF
-6.9±2 %/min
n=7
3.6±0.7 %/min
120 s
nS
50
0
TEA$_o$
Cs$_o$
TEA$_o$

Figure 13

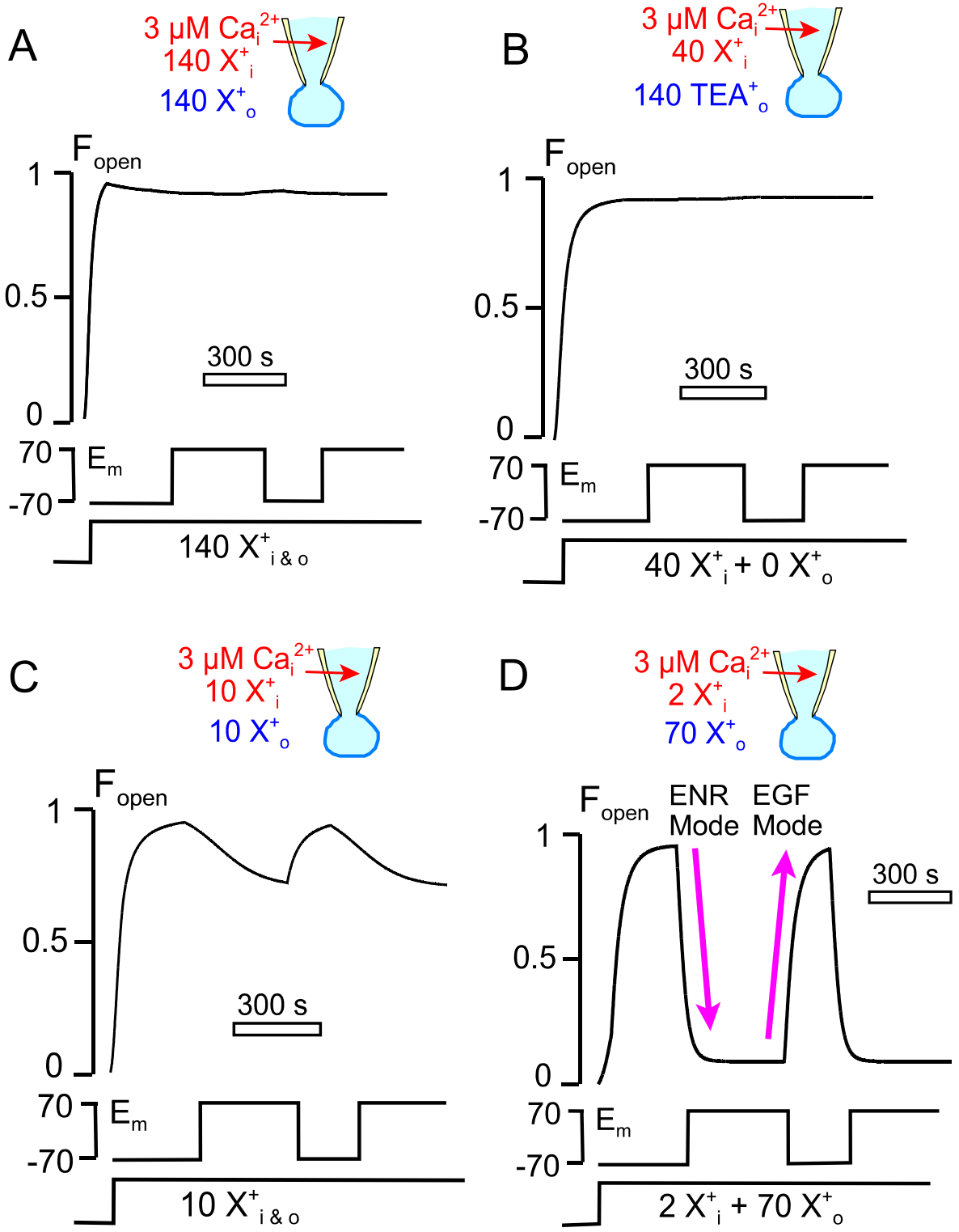

'X'=Na, K, or Cs 'ENR'= Electroneutral Reverse 'EGF'=Electrogenic Forward
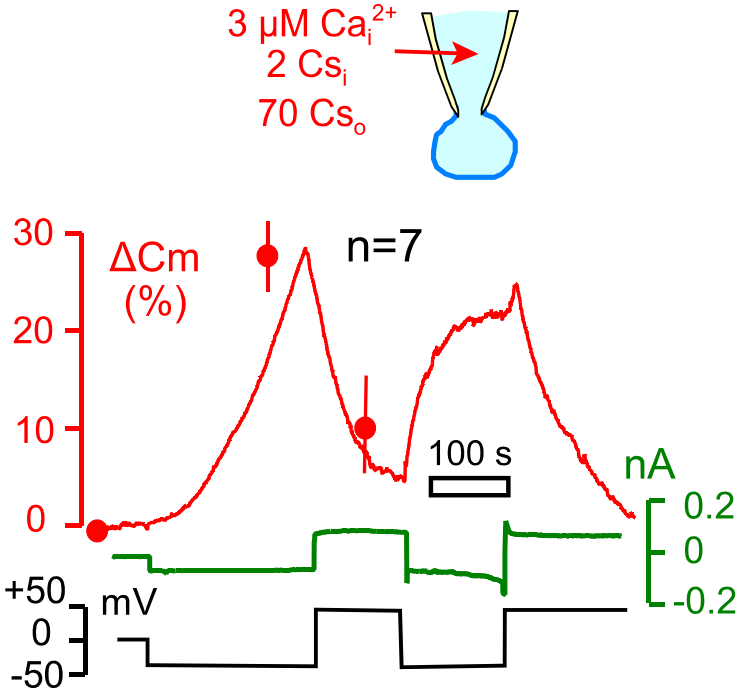
Figure 14